Textures and Microstructures, 1988, Vols. 8 & 9, pp. 267–311
Reprints available directly from the publisher
Photocopying permitted by license only

Printed in the United Kingdom

The Influence of Non-Octahedral Slip on Texture Development in FCC Metals

B. BACROIX* and J. J. JONAS

Department of Metallurgical Engineering, McGill University, 3450 University St., Montreal, H3A 2A7, Canada

(*Received March 17, 1987; in final form June 13, 1987*)

Dedicated to the memory of Professor Günter Wassermann

In order to account for the differences observed between low and high temperature deformation textures, the influence of slip or cross-slip on planes other than the {111} is considered in FCC metals. The first set of possible new slip systems treated is the {100}⟨110⟩. The dual single crystal yield surface is constructed using a novel technique, and deformation textures are predicted for rolling and torsion using the FC-RC model usually employed at room temperature. The {112} and {110}⟨110⟩ cross-slip systems are also considered. The rolling textures obtained when slip and cross-slip or only cross-slip occur are presented. These two cases are first treated on the assumption of a constant CRSS on all systems and then with the aid of a linear latent hardening law, which only takes into account the interactions between colinear systems.

It is shown that the concurrent activation of both slip and cross-slip systems leads to the presence of three main rolling components: i.e. the Cu, S and brass orientations, in proportions that vary with the CRSS ratios of the different systems. These results are in good agreement with experimental observations for high SFE metals such as aluminum. Some torsion textures are also presented for the case when both slip and cross-slip systems are activated. The trends observed in this case are not as clear as in the case of rolling. However, the B/$\bar{\text{B}}$ orientation, which is the only component found at high temperatures and high strains in aluminum, is present in higher proportions than with the classical FC-RC model, but some other texture components are also present.

KEY WORDS: Plastic deformation, rolling, torsion, texture development, Taylor model, full constraints, relaxed constraints, FCC metals, non-octahedral slip.

* Now at: Institut de Recherches de la Sidérurgie française, 185 rue du Président Roosevelt, 78105 St Germain en Laye, France.

1 INTRODUCTION

During the cold rolling of fcc metals, a copper-type texture is generally observed in high SFE materials, whereas a brass-type texture is normally formed in low SFE metals. These observations are usually interpreted in terms of enhanced cross-slip in the former case and the occurrence of twinning (Barrett and Massalski, 1966; Hu, Cline and Goodman, 1966; Grewen and Wasserman, 1969; Hirsch, 1984; Mecking, 1985) or of Sachs type deformation (Leffers, 1981) in the latter instance. As the SFE is increased, a smooth transition is observed between the two types of components. Such behaviour can be reasonably well simulated by means of the classical Taylor (or "full constraint") model for equiaxed grains (Taylor, 1938) and the relaxed constraint (or RC) model for elongated grains (Honneff and Mecking, 1978), with the assumption that the deformation is accommodated by slip on the $\{111\}\langle 110\rangle$ systems, supplemented by the occurrence of twinning. It has also been demonstrated by Smallman (1975) that low SFE materials deformed at high temperatures behave much as high SFE metals deformed at room temperature. This can be explained by the gradual disappearance of twinning as the temperature is increased. However, the influence of deformation temperature on texture development in *high SFE metals* is not well understood, in part because the effect is relatively small.

Recently, a careful examination of published experimental data has established that there is a *second* transition as the temperature is increased, in this case from the copper back to the brass-type of texture (Bacroix and Jonas, 1987a). The combined influence of temperature and SFE on texture development just described is represented schematically in Figure 1, together with the definitions of what is meant by the brass-type texture for rolling, torsion and tension (Bacroix and Jonas, 1987a). The texture transitions shown in Figure 1 can be attributed to differences in the relative ease of cross-slip, the activation of new slip or cross-slip systems, or the occurrence of dynamic recovery (Bacroix, 1986). This paper is mainly concerned with only one of these possibilities, i.e. the activation of new slip or cross-slip systems.

When the temperature is increased, the critical resolved shear stress of the $\{111\}\langle 110\rangle$ systems decreases. It is possible for the

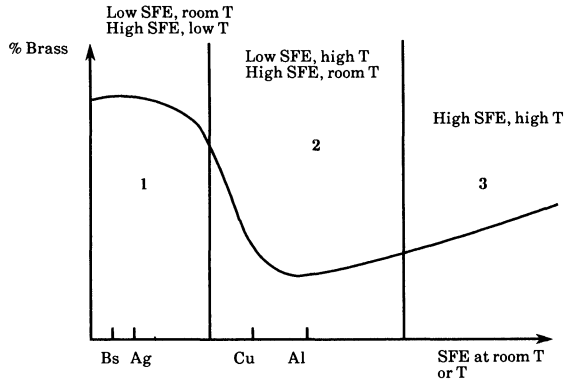

	Brass-Type	Copper-Type
Tension	<100> fibre	<111> fibre
Rolling	α fibre = Bs={110}<112> + Goss={110}<100>	β fibre = Cu={112}<111> + S={123}<634> + Bs={110}<112>
Torsion	mostly B={112}<110>	mostly C={100}<110>

Figure 1 Schematic representation of the dependence of the deformation texture of fcc materials on SFE and temperature. The brass type is described in the table included in the figure (Bacroix and Jonas, 1987a).

CRSS of other slip systems to decrease sufficiently over the same interval that these also become activated. The most probable ones in fcc metals are the $\{100\}\langle 110\rangle$, because the $\{100\}$ planes are the most densely packed after the $\{111\}$. The activation of these systems has in fact been observed at elevated temperatures (Hirth and Lothe, 1968). Slip on the $\{110\}$ and $\{112\}$ planes has also been reported in aluminum deformed above $0.35\,T_f$ (Le Hazif, Dorizzi and Poirier, 1973; Le Hazif and Poirier, 1975). Slip on planes other than the $\{111\}$ was interpreted in these cases in terms of cross-slip from a $\{111\}$ to a $\{110\}$ or $\{112\}$ plane, especially in the instances where all the $\{111\}$ planes were equally stressed and where cross-slip from one $\{111\}$ plane to another was not favored. This is the case for most of the stable experimental orientations in torsion and rolling, which is why the assumption that cross-slip takes place solely on the $\{111\}$ planes only leads to small changes in the

predicted textures (Bacroix and Jonas, 1987a). $\{100\}\langle 110\rangle$ slip can also be interpreted in terms of cross-slip, in this case from one given $\{111\}$ plane to another, resulting in apparent slip on a $\{100\}$ plane.

In this paper, the influence of new slip or cross-slip systems will be considered first separately and then concurrently with the introduction of certain hardening laws. Some rolling and torsion textures will be calculated according to the FC-RC model developed by Tomé and co-workers (1984) where a statistical transition from FC to RC conditions is performed in each grain as the deformation proceeds.† Thus, in the case of rolling, two shear components can be relaxed, whereas in torsion only one shear component is allowed to differ from grain to grain (Kocks and Canova, 1981). The analysis will be presented in five sections, which deal with the following items:

i) The construction and description of the dual $\{111\} + \{100\}$ yield surface.

ii) Some texture predictions for the cases of rolling and torsion using the dual yield surface.

iii) The activation of $\{110\} + \{112\}\langle 110\rangle$ cross-slip systems; in this section, various values of the critical resolved shear stress (CRSS) of the different types of cross-slip systems are considered and some results obtained for rolling are presented.

iv) The effect of "latent" hardening; the latter is introduced in a simple way to account for the possible occurrence of cross-slip on $\{110\}$ and $\{112\}$ planes as well as of slip on $\{100\}$ planes. Here the results are again restricted to the case of rolling.

v) The application of methods iii) and iv) above to the case of

† This approach is based on the argument that different numbers of slip systems are required in different parts of each grain, and that the volume fraction of each region changes as the strain is increased. Tomé *et al.* (1984) proposed that the volume fractions within individual grains in which 3, 4 or 5 strain components are imposed be interpreted as fractions of all the grains in the population. In this way, in rolling, all the grains start to deform according to the FC model and, as the deformation proceeds, the number of grains in which $\dot{\varepsilon}_{13}$ then $\dot{\varepsilon}_{13}$ *and* $\dot{\varepsilon}_{23}$ are relaxed increases (1, 2 and 3 refer to the rolling, transverse and normal directions, respectively). Similarly, in torsion, all the grains start to deform according to the FC mode, but only one shear component is relaxed, i.e. $\dot{\varepsilon}_{RY}$ in an increasing number of grains. Here R, X and Y designate the principal axes of current strain which coincide with R, θ, Z at infinite strain.

torsion; in this section, the torsion and rolling results are also evaluated, and the validity of the starting model is discussed.

2 THE COMPOSITE $\{111\} + \{100\}$ YIELD SURFACE

The geometric features of the 6 $\{100\}\langle 110\rangle$ systems are listed in Table 1, together with those of the 24 $\{111\}\langle 110\rangle$. This table includes the coordinates of all the systems considered here. The latter are defined in an orthonormal five dimensional space in which the deviatoric stress and strain rate tensors are represented by the following vectors (Lequeu *et al.*, 1987):

$$S = \left(\frac{(S_{22} - S_{11})}{\sqrt{2}}, \sqrt{3/2}S_{33}, \sqrt{2}S_{23}, \sqrt{2}S_{31}, \sqrt{2}S_{12}\right)$$
$$\dot{\varepsilon} = \left(\frac{(\dot{\varepsilon}_{22} - \dot{\varepsilon}_{11})}{\sqrt{2}}, \sqrt{3/2}\dot{\varepsilon}_{33}, \sqrt{2}\dot{\varepsilon}_{23}, \sqrt{2}\dot{\varepsilon}_{31}, \sqrt{2}\dot{\varepsilon}_{12}\right) \quad (1)$$

Table 1 Coordinates of the 36 slip systems associated with the composite yield surface

System no. *i.*	Slip plane n	Slip dir. b	Coordinates of N^i				
			m_1	m_2	m_3	m_4	m_5
1–13	$11\bar{1}$	011	$1/2\sqrt{3}$	$-1/2$	0	$1/2\sqrt{3}$	$1/2\sqrt{3}$
2–14	$11\bar{1}$	101	$-1/2\sqrt{3}$	$-1/2$	$1/2\sqrt{3}$	0	$1/2\sqrt{3}$
3–15	$11\bar{1}$	$1\bar{1}0$	$-1/\sqrt{3}$	0	$1/2\sqrt{3}$	$-1/2\sqrt{3}$	0
4–16	$1\bar{1}\bar{1}$	$01\bar{1}$	$-1/2\sqrt{3}$	$1/2$	0	$-1/2\sqrt{3}$	$1/2\sqrt{3}$
5–17	$1\bar{1}\bar{1}$	101	$-1/2\sqrt{3}$	$-1/2$	$-1/2\sqrt{3}$	0	$-1/2\sqrt{3}$
6–18	$1\bar{1}\bar{1}$	110	$-1/\sqrt{3}$	0	$-1/2\sqrt{3}$	$-1/2\sqrt{3}$	0
7–19	$1\bar{1}1$	011	$-1/2\sqrt{3}$	$1/2$	0	$1/2\sqrt{3}$	$1/2\sqrt{3}$
8–20	$1\bar{1}1$	$10\bar{1}$	$-1/2\sqrt{3}$	$1/2$	$1/2\sqrt{3}$	0	$-1/2\sqrt{3}$
9–21	$1\bar{1}1$	110	$-1/\sqrt{3}$	0	$1/2\sqrt{3}$	$1/2\sqrt{3}$	0
10–22	111	$01\bar{1}$	$1/2\sqrt{3}$	$-1/2$	0	$-1/2\sqrt{3}$	$1/2\sqrt{3}$
11–23	111	$10\bar{1}$	$-1/2\sqrt{3}$	$-1/2$	$-1/2\sqrt{3}$	0	$1/2\sqrt{3}$
12–24	111	$1\bar{1}0$	$-1/\sqrt{3}$	0	$-1/2\sqrt{3}$	$1/2\sqrt{3}$	0
25–31	100	011	0	0	0	$1/2$	$1/2$
26–32	100	$01\bar{1}$	0	0	0	$-1/2$	$1/2$
27–33	010	101	0	0	$1/2$	0	$1/2$
28–34	010	$10\bar{1}$	0	0	$-1/2$	0	$1/2$
29–35	001	110	0	0	$1/2$	$1/2$	0
30–36	001	$1\bar{1}0$	0	0	$-1/2$	$1/2$	0

The normal to the facet corresponding to system i is defined by the following N^i vector:

$$N^i = \left(\frac{(n_2^i b_2^i - n_1^i b_1^i)}{\sqrt{2}}, \sqrt{3/2} n_3^i b_3^i, \right.$$
$$\left. \frac{\sqrt{2}}{2}(n_2^i b_3^i + n_3^i b_2^i), \frac{\sqrt{2}}{2}(n_1^i b_3^i + n_3^i b_1^i), \frac{\sqrt{2}}{2}(n_1^i b_2^i + n_2^i b_1^i) \right) \quad (2)$$

where n^i and b^i are the slip plane normal and slip direction defining system i. It should first be noted that the $\{100\}\langle 110\rangle$ systems are not independent 5 by 5 (i.e., their first two components are all equal to zero), which means that they cannot by themselves accommodate any imposed strain rate vector.

In order to be able to perform Bishop and Hill calculations (i.e. using the principle of maximum work), the possible stress states (coordinates of the vertices of the composite yield surface) must be known. These vertices can be characterized by considering all the combinations of 5 out of the full 36 slip systems (defined in terms of N^i) and determining if there exists a solution to the following linear problem:

$$\begin{aligned} S \cdot N^i &= \tau_c^i \quad \text{for} \quad i = 1, 5 \\ S \cdot N^i &\leq \tau_c^i \quad \text{for the others} \end{aligned} \quad (3)$$

Here S is normalized by the CRSS of the $\{111\}\langle 110\rangle$ systems such that $\tau_{c1} = 1$ for the $\{111\}\langle 110\rangle$ and $\tau_{c2} = \alpha$ for the $\{100\}\langle 110\rangle$. If the determinant of this set of equations differs from zero, then the systems under consideration are independent and it is possible to define a stress state that activates them. This involves a considerable amount of computing time, which can be reduced if the method developed by Tomé and Kocks (1985) is used. The latter technique is completely general, can be used for any structure, and is very efficient when nothing is known a priori about the yield surface.

In the present case, another method was employed (based on that of Tomé and Kocks) which takes advantage of the detailed knowledge available of the classical Bishop and Hill yield surface. This method is more elegant and still reduces the computing time. The coordinates of all the vertices, 4th, 3rd and 2nd order edges of the conventional BH yield surface were tabulated by Kocks, Canova and Jonas (1983). With this information available, it is

possible to derive analytically the locations of the vertices of the new SCYS by determining where the planes associated with the new systems, i.e. the $\{100\}\langle 110\rangle$ ones, intersect the BH polyhedron. But first, the range of variation of α must be defined; the latter represents $1/\sqrt{2}$ of the distance of a given $\{100\}\langle 110\rangle$ plane from the origin of the yield surface† (when the stress states are normalized by τ_{c1}, the CRSS of the $\{111\}\langle 110\rangle$ systems). If α is such that none of the vertices of the BH polyhedron is eliminated by the addition of the new systems, the yield surface remains unchanged and the new slip systems are never activated. Thus, every stress state of the BH polyhedron which satisfies the relation:

$$S_{BH} \cdot N^j > \alpha \tag{4}$$

for at least one of the 12 $\{100\}\langle 110\rangle$ systems (indexed j), lies outside the new yield surface. The points of intersection can be located on the facets of this YS (where only one $\{111\}\langle 110\rangle$ system is activated), or on the edges (where 2 to 6 are activated) or even at the vertices. They constitute new vertices if they activate at least 5 independent systems. The facets are readily eliminated, since they involve the activation of 4 $\{100\}\langle 110\rangle$ systems, which are not independent 4 by 4.

2.1 Construction of the composite yield surface

General procedure. Let us now consider the vertices of the BH polyhedron. To determine whether or not these are retained by the cutting procedure, the products $S^i \cdot N^j$ were calculated for each of the 28 stress states S^i of the BHYS and every N^j vector associated with each of the 6 (plus opposite) $\{100\}\langle 110\rangle$ systems. The results of this calculation are listed in Table 2. It can readily be seen that if α is greater than $\sqrt{3}$, the new systems never intersect the BHYS. For α ranging from $\sqrt{3}$ to $\sqrt{3/2}$, some vertices are retained and

† The distance from the origin of a given plane of normal N^j is expressed by:

$$d = S \cdot N^j / \|N^j\| = 1/\|N^j\| = \sqrt{2} \text{ for the } \{111\}\langle 110\rangle \text{ systems}$$
$$= \alpha/\|N^j\| = \alpha\sqrt{2} \text{ for the } \{100\}\langle 110\rangle \text{ systems.}$$

This is because, in the 5 dimensional space defined here, the N^j vectors are *not* unit vectors (see Eq. 2); instead, their norms are given by $\|N^j\| = 1/\sqrt{2}$.

Table 2 Value of the product $S^i \cdot N^j$ for the 28 vertices of the BH polyhedron and the $6\{100\}\langle 110\rangle$ systems

Group	Vertex no. i.	$S^i \cdot N^j$ for the 28 vertices and the 6 new systems (normalized by $\sqrt{3}$)					
		$S^i \cdot N^{25}$	$S^i \cdot N^{26}$	$S^i \cdot N^{27}$	$S^i \cdot N^{28}$	$S^i \cdot N^{29}$	$S^i \cdot N^{30}$
A	1	0	0	0	0	0	0
	2	0	0	0	0	0	0
	3	0	0	0	0	0	0
B	4	1	0	1	0	1	0
	5	1	0	0	1	0	1
	6	0	1	1	0	0	−1
	7	0	−1	0	−1	1	0
C	8	0	0	1	−1	1	−1
	9	1	−1	0	0	1	1
	10	1	1	1	1	0	0
D	11	1	0	1/2	1/2	1/2	1/2
	12	−1	0	−1/2	−1/2	−1/2	−1/2
	13	0	−1	−1/2	−1/2	1/2	1/2
	14	0	1	1/2	1/2	−1/2	−1/2
	15	1/2	1/2	1	0	1/2	−1/2
	16	−1/2	−1/2	−1	0	−1/2	1/2
	17	1/2	1/2	0	1	−1/2	1/2
	18	−1/2	−1/2	0	−1	1/2	−1/2
	19	1/2	−1/2	1/2	−1/2	1	0
	20	−1/2	1/2	−1/2	1/2	−1	0
	21	−1/2	1/2	1/2	−1/2	0	−1
	22	1/2	−1/2	−1/2	1/2	0	1
E	23	0	0	1/2	−1/2	1/2	−1/2
	24	0	0	−1/2	1/2	−1/2	1/2
	25	1/2	−1/2	0	0	1/2	1/2
	26	−1/2	1/2	0	0	−1/2	−1/2
	27	1/2	1/2	1/2	1/2	0	0
	28	−1/2	−1/2	−1/2	−1/2	0	0

others are eliminated by at least one new system. For α less than $\sqrt{3/2}$, a completely new configuration exists. However, the last case is not of interest because it would signify that the $\{100\}\langle 110\rangle$ systems are more easily activated than the $\{111\}\langle 110\rangle$, which is unrealistic. It thus remains to examine only the case where

$$\sqrt{3/2} < \alpha < \sqrt{3} \tag{5}$$

From Table 2 it is evident that, for this specific range of α, the type A and E vertices still lie on the "dual" yield surface, whereas those of types B, C and D are eliminated. Turning now to the

edges, it can readily be determined whether a particular edge is retained completely, only partly, or eliminated entirely when the surface is cut by new planes. In this procedure, it is sufficient to consider only one edge of each type because of the cubic symmetry. All the other edges of the same type (i.e. 4A to 4H, 3A to 3G and 2A to 2E) can be deduced from the first by applying symmetry operations. Furthermore, if a new vertex is found on a particular edge, the vertices associated with the other edges of the same group can also be found by applying the symmetry operations to the first vertex.

If all the vertices delimiting one particular edge are eliminated by at least one of the new systems, then the complete edge is eliminated as well. Examining all the different types of edges, it can be said without any further calculation and simply by looking at the values of the product $S^i \cdot N^j$ that the 4C, 4D, 4E, 4F, 3D, 3E and 2B edges do not belong to the new yield surface and only the remaining edges need be considered further. In this way, it can also be shown that all of the type 4B and 3B edges are retained. The other ones are only partly retained. It is thus now necessary to look at a representative example of each of the following groups: 4A, 4G, 4H, 3A, 3C, 3F, 3G, 2A, 2C, 2D and 2E, and to determine the new vertices which lie on these edges.

To do so, advantage can be taken of still another property of the BH yield surface, i.e. that each nth order edge is delimited by edges of higher order. For example, a 4th order edge constitutes a one dimensional space and is delimited by 2 vertices. (These are points in 5 dimensional space and thus have no dimension.) A 3rd order edge constitutes a two dimensional surface and is delimited by 3 or 4 vertices defining 3 or 4 4th order edges. Similarly, a 2nd order edge, surrounded by 5, 6 or 8 vertices, constitutes a 3 dimensional volume, whose faces are 3rd order edges and whose edges are 4th order edges (see Figure 2). It is therefore possible to consider only the 2nd order edges (more specifically one of each type), since they include all the possible types of 3rd and 4th order edges, and determine on these where the planes associated with the new systems intersect to create vertices.

The problem can in this way be reduced to the following. Which stress states included in the volume of one particular second order edge are part of the new YS, and which ones activate at least 5 independent slip systems so as to constitute a vertex?

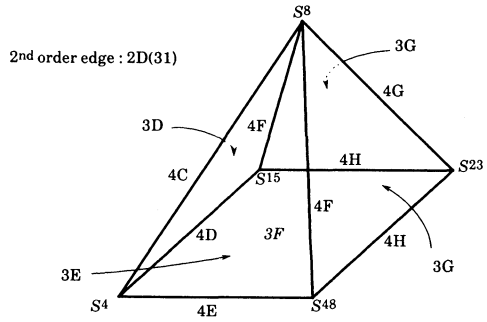

Figure 2 Example of a second order edge (notation of Kocks, Canova and Jonas, (1983)).

If 3 planes associated with the $\{100\}\langle 110\rangle$ systems intersect at a point within the volume defined by the edge, this point constitutes a vertex since 2 $\{111\}\langle 110\rangle$ systems are already activated at this point; this situation nevertheless requires that:

1) the 5 systems be independent; and that
2) the stress state considered satisfies the relation $S \cdot N^j \leqq \alpha$ for all the other $\{100\}\langle 110\rangle$ systems.

If 2 planes intersect at a point of a 3rd order edge (a facet of the 2nd order edge), this point is also a vertex, since 3 systems are already active at this point (provided that the above 2 conditions are again fulfilled). The same holds if a plane intersects a 4th order edge. The two conditions listed above have to be checked every time a new vertex is being tested.

Example. Let us now consider a specific example to describe the complete procedure. Second order edge number 31 of type 2D is delimited by vertices 4, 8, 15, 23 and 48 in the notation of Kocks, Canova and Jonas (1981) and is represented schematically in Figure 2, together with the associated edges of 3rd and 4th order. It is already known that, among these particular edges, only the 4G, 4H, 3F, 3G and 2D are partly retained, the others being completely eliminated. These edges can thus be examined one by one to establish the actual intersection points.

i) *Edge* $4G$: This edge is delimited by vertices 8 and 23 and activates systems 2, 8, 18 and 24. Every stress state lying on this edge satisfies the relation:

$$S = \alpha_1 S^8 + \alpha_2 S^{23} \tag{6}$$

with

$$\alpha_1 + \alpha_2 = 1 \quad \text{and} \quad \alpha_1,\ \alpha_2 \geq 0$$

From Table 2, it can be seen that systems 27, 29, 34 and 36 intersect this edge. Calculating the product $S \cdot N_j$ for these 4 systems gives:

$$\begin{aligned} S \cdot N^{27} &= \sqrt{3}(\alpha_1 + \alpha_2/2) \\ S \cdot N^{29} &= \sqrt{3}(\alpha_1 + \alpha_2/2) \\ S \cdot N^{34} &= \sqrt{3}(\alpha_1 + \alpha_2/2) \\ S \cdot N^{36} &= \sqrt{3}(\alpha_1 + \alpha_2/2) \end{aligned} \tag{7}$$

If one of these products is equal to α, the corresponding stress state constitutes a vertex of the new yield surface (provided that the independence of the systems is satisfied). It is readily seen that for:

$$S = S^8 + \beta(S^{23} - S^8) \quad \text{with} \quad \beta = 2(1 - \alpha/\sqrt{3}) \tag{8}$$

the 4 systems are critical and this point constitutes a vertex of the yield surface associated with the 8 systems: 2, 18, 8, 24, 27, 29, 34 and 36 ($4\{111\}\langle 110\rangle$ and 4 $\{100\}\langle 110\rangle$ systems). This of course requires that a combination of 5 independent systems can be found among the 8, a matter which will be checked later.

ii) *Edge* $4H$: This edge is defined by vertices 48 and 23 and is associated with the 5 slip systems 1, 2, 8, 16, and 18. When the above procedure is repeated, it is found that the stress state:

$$S = S^{48} + \beta(S^{23} - S^{48}) \quad \text{with} \quad \beta = 2(1 - \alpha/\sqrt{3}) \tag{9}$$

activates the following 6 systems: 1, 2, 8, 16, 18 and 35 (i.e. 5 $\{111\}\langle 110\rangle$ systems $+1\{100\}\langle 110\rangle$).

iii) *Edge* $3F$: This edge is defined by vertices 4, 15, 23 and 48 and is associated with systems 1, 2 and 18. When the two groups of vertices 4, 15, 48 and 4, 23, 48 are investigated separately, a vertex is found which fulfills the condition:

$$S = S^4 + \beta(S^{23} - S^4) \quad \text{with} \quad \beta = 2(1 - \alpha/\sqrt{3}) \tag{10}$$

It activates 3 $\{111\}\langle 110\rangle$ systems (1, 2 and 18) and two $\{100\}\langle 110\rangle$ systems (27 and 29).

Edges 3G and 2B were also investigated in this way, but no new vertex was found within these edges and this study is not reproduced here. The above procedure was then repeated for a representative example of each second order edge of types 2A, 2C and 2E to enable all the vertices of the yield surface to be determined analytically.

2.2 Description of the composite $\{111\} + \{100\}$ yield surface

The procedure described above leads to the determination of the stress states which activate at least 5 systems among the 36 available. It remains to be checked if, among the 5, 6 or 8 found, it is possible to find 5 which are independent. This has been done with the aid of a computer and it was found in this way that the new yield surface is composed of 93 vertices divided into 8 groups. These are defined in Table 3, which gives the vertices or edges of the BH yield surface on which these new vertices are located, the number of vertices in each group, as well as the number of combinations of 5 independent systems associated with each vertex. Also included are the coordinates of one representative of each group.

It should be noted that for 21 vertices out of 93, the extent of the ambiguities is expected to be large (32, 36 or 40 combinations are possible), whereas for the 72 others, there is only one possible combination of 5 independent slip systems.

The 4th order edges can now be derived, so as to have an idea of the ambiguities present in an RC calculation. These edges were determined by the method of Kocks, Canova and Jonas (1981); i.e. by examining the connections between vertices and testing whether these pairs activate at least four common slip systems. The independence of the systems also has to be verified. A similar procedure was used to determine the 3rd order edges and the results for the two sets of edges are presented in Tables 4 and 5, respectively. It can be seen that the composite YS comprises 288 4th order edges associated with 672 combinations of 4 independent systems and 310 3rd order edges associated with 364 combinations of 3 independent systems. The procedure described in this para-

Table 3 Types of vertices making up the composite yield surface

Type	BH edge or vertex	Types of slip plane	No. of vertices	No. of comb. of 5 indep. systems	Coordinates of vertex σ^i as a function of α					Norm of S^i	Associated systems
					S_1	S_2	S_3	S_4	S_5		
I	5A	8{111}	3	32×3^b	$-\sqrt{3}$	-1	0	0	0	2	2–3–5–6–8–9–11–12
II	5E	8{111}	6	36×6^b	$\sqrt{3}/2$	$-3/2$	$\sqrt{3}$	0	0	$\sqrt{6}$	1–2–8–10–16–18–19–24
III	4A	4{111} + 4{100}	6	40×6^b	$\alpha-\sqrt{3}$	$\alpha/\sqrt{3}-1$	2α	0	0	2.17	2–3–8–9–27–29–34–36
IV	4G	4{111} + 4{100}	6	40×6^b	$\sqrt{3}-\alpha$	$\alpha\sqrt{3}-3$	2α	0	0	2.48	2–8–18–24–27–29–34–36
V	4H	5{111} + 1{100}	24	4×24^b	$\alpha-1.5\sqrt{3}$	$0.5-\alpha/\sqrt{3}$	0	$2\alpha-\sqrt{3}$	$\sqrt{3}$	2.37	2–7–9–11–12–25
VI	3F	3{111} + 2{100}	24	1×24	$2(\alpha-\sqrt{3})$	0	$2\alpha-\sqrt{3}$	$2\alpha-\sqrt{3}$	$\sqrt{3}$	2.30	2–7–9–25–27
VII	2A	2{111} + 3{100}	12	1×12	$\alpha-\sqrt{3}$	$\alpha/\sqrt{3}-1$	α	$-\alpha$	α	1.93	2–3–26–27–36
VIII	2C	2{111} + 3{100}	12	1×12	$\alpha-\sqrt{3}$	$\alpha/\sqrt{3}-1$	α	α	α	1.93	2–9–25–27–29
Totals			93[a]	936[a]							

[a] Plus their opposites
[b] Ambiguities present

Table 4 Number of combinations of four independent slip systems under tetraslip ($p = 4$) conditions in the composite yield surface

Type of edge and no. of associated slip systems (n)	Types of slip plane	Types of connecting vertices	Number of edges of given type	Total number of comb. of 4 systems per edge	Number of comb. of 4 independent systems	Example of edge	
						Connecting Vertices	Associated systems
4A(6)	6{111}	I–II	12	15	12×12[b]	1–8	2–3–6–11–12
4B(4)	4{111}	I–III	6	1	1×6	1–10	2–3–8–9
4C(4)	4{111}	II–IV	6	1	1×6	4–16	2–8–18–24
4D(5)	5{111}	II–V	24	5	4×24[b]	8–22	2–7–9–11–12
4E(6)	2{111} + 4{100}	III–IV	12	15	13×12[b]	10–16	2–8–27–29–34–36
4F(4)	3{111} + 1{100}	III–V	24	1	1×24	10–126	2–3–9–27
4G(4)	2{111} + 2{100}	III–VII	12	1	1×12	10–70	2–3–27–36
4H(4)	2{111} + 2{100}	III–VIII	12	1	1×12	13–76	10–24–26–36
4I(4)	3{111} + 1{100}	IV–V	24	1	1×24	16–30	2–18–24–27
4J(4)	2{111} + 2{100}	IV–VI	24	1	1×24	16–49	2–18–27–29
4K(5)	4{111} + 1{100}	V–V	12	5	4×12[b]	22–23	2–9–11–12–25
4L(4)	3{111} + 1{100}	V–VI	48	1	1×48	22–46	2–7–9–25
4M(4)	2{111} + 2{100}	VI–VII	24	1	1×24	58–70	2–3–26–27
4N(4)	2{111} + 2{100}	VI–VIII	24	1	1×24	46–82	2–9–25–27
4O(4)	1{111} + 3{100}	VII–VIII	24	1	1×24	70–180	3–26–27–36
Totals			288[a]		672[a]		

[a] Plus their opposites.
[b] Ambiguities present.

Table 5 Number of combinations of three independent slip systems under trislip ($p = 3$) conditions in the composite yield surface.

Type of edge and no. of associated slip systems (n)	Types of slip plane	Types of connecting vertices	Number of edges of given type	Number of comb. of 3 independent systems	Example of edge	
					Connecting vertices	Associated systems
3A(3)	3{111}	I–II–III–V	24	1×24	1–8–10–126	2–3–9
3B(4)	4{111}	I–II–I–II	3	4×3[b]	1–8–9–95	2–6–9–12
3C(4)	4{111}	II–I–II–V–V	12	4×12[b]	1–8–28–29–99	2–3–6–11
3D(3)	3{111}	II–V–V–VI	24	1×24	8–22–46–126	2–7–9
3E(3)	3{111}	II–IV–V	24	1×24	4–16–30	2–18–24
3F(4)	4{100}	III–III–IV–IV	3	4×3[b]	10–16–17–104	27–29–34–36
3G(3)	2{111} + 1{100}	III–IV–V–V	24	1×24	10–17–125–126	3–9–27
3H(3)	1{111} + 2{100}	III–IV–VI–VII–VIII	48	1×48	10–16–61–70–185	2–27–36
3I(3)	2{111} + 1{100}	III–V–VI–VII	48	1×48	10–58–70–126	2–3–27
3J(3)	3{100}	VII–VIII–VII–VIII–VII–VIII	4	1×4	70–76–79–178–180–185	26–27–36
3K(3)	2{111} + 1{100}	V–V–VI–VI–VII	24	1×24	28–29–58–59–70	2–3–26
3L(3)	1{111} + 2{100}	VI–VII–VIII	24	1×24	58–70–180	3–26–27
3M(3)	2{111} + 1{100}	IV–V–VI	48	1×48	16–30–49	2–18–27
Totals			310[a]	364[a]	364[a]	

[a] Plus their opposites.
[b] Ambiguities present.

graph has also been applied with success to the construction of a mixed yield surface for bcc materials (Orlans-Joliet *et al.*, 1987).

3 FC-RC PREDICTIONS FOR THE CASE OF DUPLEX SLIP

It was first checked that the extent of the ambiguities in terms of rotations was small in the case of torsion and rolling for both the FC and FC-RC models (see Section 1 for the description of the FC-RC model). Whenever there were several solutions, the average rotation was calculated. The influence of the α parameter was also investigated. It is worth noting that the value of α has no influence on the FC predictions as long as it remains in the range defined above. Although it affects the *stress state,* the activated slip systems remain the same. However, in an RC calculation, even if the vertices are associated with the same systems for different values of α, a plane $S_4 = 0$ (for example) can cut the yield surface in different places for different values of α, resulting in the activation of different sets of slip systems. So the value of α does have an influence on FC-RC simulations.

The FC-RC predictions obtained for torsion are presented in terms of {111} pole figures in Figure 3 for $\alpha = 1.5$ and in Figure 4 for $\alpha = 0.89$. These two values are located at the two extremes of the allowable range. For $\alpha = 1.5$, the $\{100\}\langle 110\rangle$ systems cut the BHYS only slightly, so that the predictions are close to the classical FC-RC ones. The $A/\bar{A}$, $B/\bar{B}$ and C components are present in the same proportions:† C is the strongest at large strains, followed by $A/\bar{A}$, whereas $B/\bar{B}$ is almost absent (Canova, Kocks and Jonas, 1984). For $\alpha = 0.89$, on the other hand, the $\{100\}\langle 110\rangle$ systems have more influence on the calculations and a new texture component appears: the $\{100\}\langle 010\rangle$, which involves the equal activation of two of the new systems. This component is the equivalent of the C orientation for the $\{111\}\langle 110\rangle$ systems, in the sense that it activates only two slip systems in a symmetrical manner. These systems are coplanar whereas the C orientation activates two colinear systems. Unfortunately, it is not observed at high tempera-

† See Figure 15 for the definition of the torsion ideal orientations, $A/\bar{A}$, $B/\bar{B}$ and C.

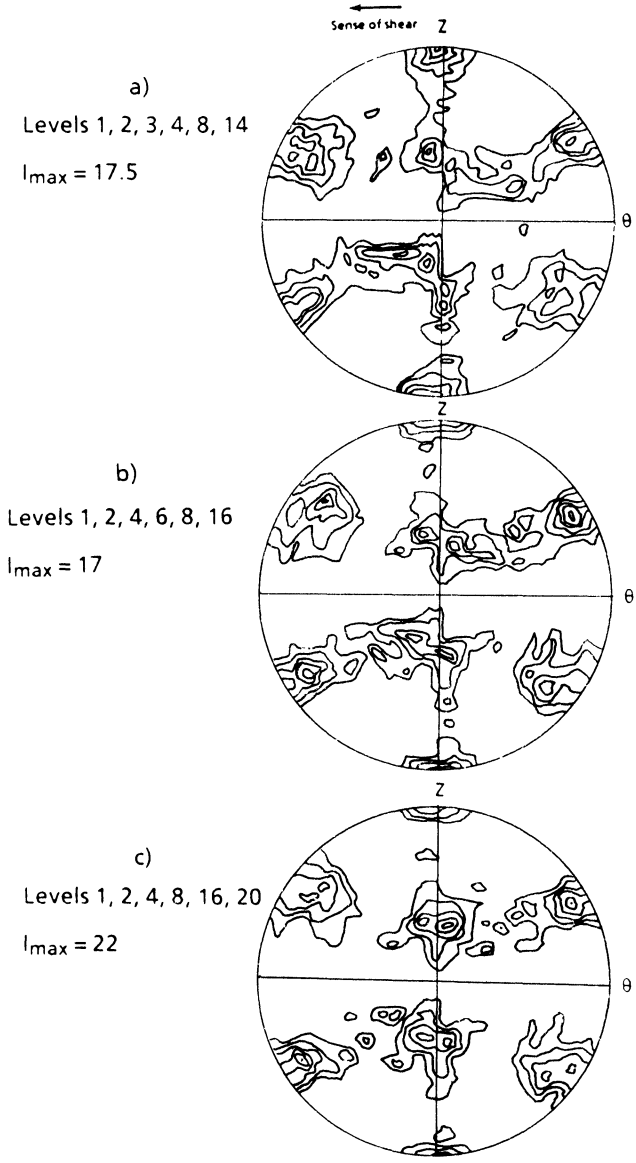

Figure 3 Torsion textures predicted using the FC-RC model with $\{111\} + \{100\}\langle 110\rangle$ slip. $\tau_{c(100)}/\tau_{c(111)} = 1.5$; a) $\bar{\varepsilon} = 2$, b) $\bar{\varepsilon} = 4$ and c) $\bar{\varepsilon} = 6$; $\{111\}$ pole figures.

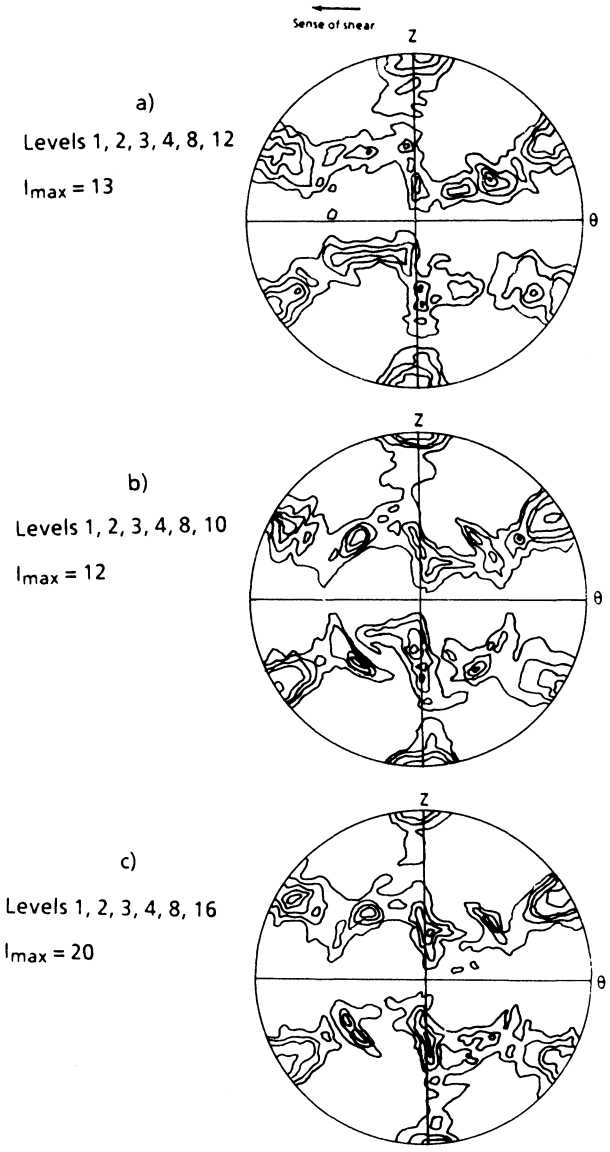

Figure 4 Torsion textures predicted using the FC-RC model with $\{111\} + \{100\}\langle 110\rangle$ slip. $\tau_{c(100)}/\tau_{c(111)} = 0.89$; a) $\bar{\varepsilon} = 2$, b) $\bar{\varepsilon} = 4$ and c) $\bar{\varepsilon} = 6$; {111} pole figures.

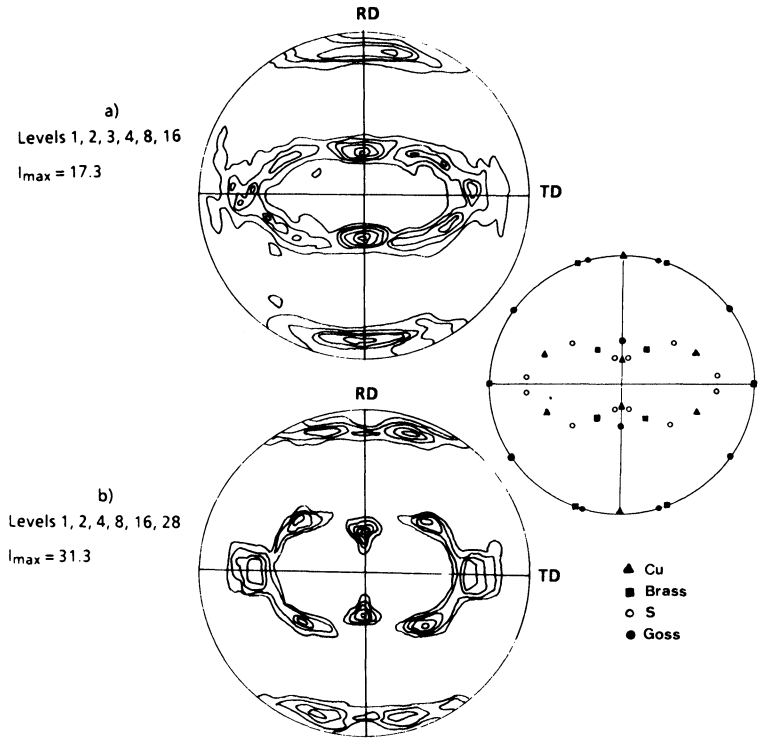

Figure 5 Rolling textures predicted using the FC-RC model with $\{111\} + \{100\}\langle 110\rangle$ slip. $\tau_{c(100)}/\tau_{c(111)} = 1$; a) $\bar{\varepsilon} = 1$ and b) $\bar{\varepsilon} = 3$; $\{111\}$ pole figures.

tures (Montheillet, Cohen and Jonas, 1984). Moreover, introduction of the $\{100\}\langle 110\rangle$ systems does not lead to an increase in the $B/\bar{B}$ component, as can be seen from Figure 4, whereas the $B/\bar{B}$ orientation is the one which becomes accentuated in aluminum at high strains (and to a lesser extent in copper) (Montheillet, Cohen and Jonas, 1984).

Some $\{111\}$ pole figures obtained for the case of rolling with $\alpha = 1$ are shown in Figure 5 for strains of 1 and 3 and Figure 6 shows the CODF corresponding to $\bar{\varepsilon} = 3$. The procedure used to calculate the ODF from the theoretical results is described in Appendix 1. A gaussian spread of 3° was generated around each of

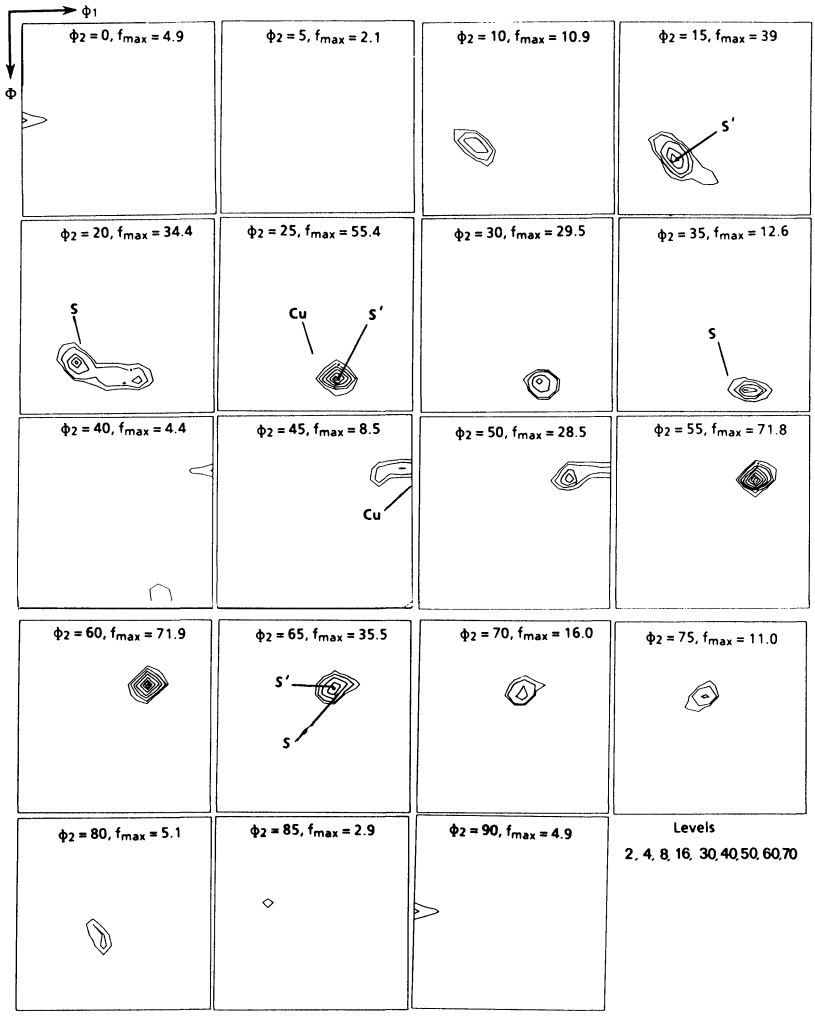

Figure 6 CODF corresponding to Figure 5b. A gaussian spread of 3° has been fitted to each of the 800 orientations composing the texture. The following legend applies to Figures 6, 8–11, 13, 14: Cu = {112}⟨111⟩; Bs = {011}⟨211⟩; S = {123}⟨634⟩; S′ = {124}⟨211⟩.

the 800 orientations used in the calculation. Even though the chosen spread is unrealistically small and the maxima obtained very sharp, the stable orientations obtained with such a dual yield surface can be identified more clearly in this way. From Figure 6, it can be seen that the activation of both the {111} and {100} slip planes produces a sharp S component, which can be described here as {124}⟨211⟩, a component which is sometimes found in aluminum (Ito, Müsik and Lücke, 1983). The copper component is much weaker and the brass component is completely absent. These results are in disagreement with the conclusions reached by Wierzbanowski (1978) who claimed that the activation of {100}⟨110⟩ systems leads to a strong copper texture (i.e., one composed of the Cu, S and brass orientations). It should be added, however, that his calculations were performed according to the strict FC model.

From these figures, it can be seen that the introduction of {100}⟨110⟩ slip does not lead to the deformation textures observed at high temperature. It was thus decided to simulate the addition of the {110}⟨110⟩ and {112}⟨110⟩ systems as well, since cross-slip on these planes has indeed been observed.

4 ACTIVATION OF THE {110} + {112}⟨110⟩ SYSTEMS

4.1 Experimental evidence

The incorporation of these systems is based on the experimental observations of Le Hazif, Dorizzi and Poirier (1973) and Le Hazif and Poirier (1975). These authors reported that slip on {110} and {112} planes is possible in fcc materials under some conditions. They compressed single crystals of Ag, Al, Au, Cu and Ni with a {100} axis parallel to the compression axis in each case. They then determined the temperatures T_1 below which only the {111} planes are active and the temperatures T_2 above which only the {110} planes are active (See Table 6). They also found that there was a nearly linear relationship between T_1 (or T_2) and $1/\gamma$ (the SFE). They interpreted their observations in terms of cross-slip from {111} to {110} planes and defined a critical resolved shear stress for cross-slip which is strongly dependent on the temperature, especially for the two types of slip plane quoted above.

Table 6 Values of the temperatures T_1 and T_2 for the materials tested in compression by Le Hazif, Dorizzi and Poirier (1973)

Metal	T_1 (K)	T_2 (K)	T_m (K)	T_1/T_m	T_2/T_m
Al	≃350	≃540	933	≃0.35	≃0.60
Ni	≃700	≃1225	1726	≃0.40	≃0.70
Au	≃650	≃900	1336	≃0.50	≃0.70
Cu	≃820	≧1270	1356	≃0.60	≧0.91
Ag	≃870	≧1185	1234	≃0.70	≧0.96

They proposed the following mechanism to account for their observations: for the particular orientation studied, deformation takes place, in the early stages, by an equal amount of slip on the 4 {111} planes. Since all the {111} are primary planes and dislocations are equally hindered on all of them, nothing would be gained by cross-slipping from one to another. The deformation can only be continued if the dislocations are able to escape onto {110} planes. Then, the glide may be stabilized on the latter by the creation of stable stacking faults on these planes. Their T_1 and T_2 temperatures for aluminum were 77 and 267°C, respectively. It can be argued that these are unreasonably low, but it must be borne in mind that they were determined for very specific orientations. For an untextured material, the equivalent average temperatures for all possible orientations can be assumed to be higher. Cross-slip from the {111} to the {112} planes was also given the same interpretation (Le Hazif, Dorizzi and Poirier, 1973).

4.2 Interpretation of the results of Le Hazif *et al*

Figure 7 is taken from the work of Chin and Mammel (1967) and shows the domains of activation of the 5 different classes of vertex pertaining to the Bishop and Hill polyhedron. The number of pairs of colinear systems associated with each of these vertex regions is also indicated on this figure. It can be seen that for all the orientations which activate vertices of type A, B or C, cross-slip from one {111} plane to another is impossible since the critical systems are already grouped into 3 or 4 pairs of colinear systems. In such cases, other cross-slip systems must become active. To check this possibility, a single orientation was chosen in each of the 5

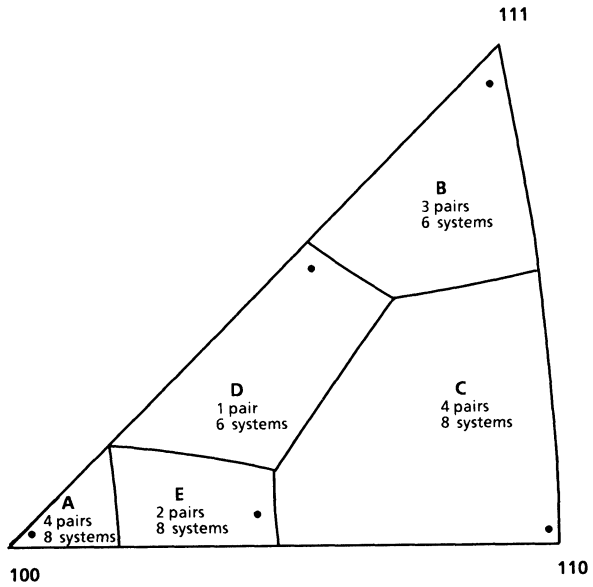

Figure 7 Number of systems and pairs of colinear systems associated with each type of vertex. The orientations considered in Section 4.2 are also represented on this figure (●).

domains (see Figure 7) and the activated slip systems were determined for different values of the CRSS's of the $\{111\}\langle 110\rangle$, $\{100\}\langle 110\rangle$, $\{110\}\langle 110\rangle$ and $\{112\}\langle 110\rangle$ systems for the case of compression. The results are presented in Table 7. It can be seen from this table that, for the particular case of the A orientation (which corresponds to the experiments of Le Hazif *et al.*), cross-slip from the $\{111\}$ to the $\{110\}$ can take place; by contrast, for the B orientation, only the $\{112\}$ or $\{100\}\langle 110\rangle$ systems can become active. It would be of interest to check this prediction experimentally by compressing a $\{111\}$ single crystal. (Note that the letters A to E refer here to the type of active vertex and do not correspond to ideal orientations.)

These calculations also provided the values of CRSS below which the different families of slip system can become active. If the CRSS of the $\{111\}\langle 110\rangle$ systems is set equal to 1, the critical values for

Table 7 Types of activated systems for the five orientations defined in Figure 7

Orientation	Possible active systems				
	{111} + {100}	{111} + {110}	{111} + {112}	{111} + {110} + {112}	{111} + {100} + {110} + {112}
A[a]	{111}	{111} + {110}	{111}	{111} + {110}	{111} + {110}
B	{111} + {100}	{111}	{112}	{112}	{100} + {112}
C	{111} + {100}	{111}	{112}	{112}	{100} + {110} + {112}
D	{111} + {100}	{111}	{111} + {112}	{111} + {112}	{111} + {100} + {110} + {112}
E	{111}	{111} + {110}	{111} + {112}	{111} + {112}	{111} + {100} + {100} + {112}

[a] Orientation near the one described by Le Hazif, Dorizzi and Poirier (1973) and Le Hazif and Poirier (1975).

the others are the following:

$$\begin{aligned} \tau_{c(110)} \leqq \sqrt{6}/2 &\Rightarrow \{110\}\langle 110\rangle \text{ active} \\ \tau_{c(112)} \leqq \sqrt{2} &\Rightarrow \{112\}\langle 110\rangle \text{ active} \\ \tau_{c(100)} \leqq \sqrt{3} &\Rightarrow \{100\}\langle 110\rangle \text{ active} \end{aligned} \tag{11}$$

It was thus decided to simulate such a cross-slip situation in rolling by first simply adding† the $\{110\}\langle 110\rangle$ and $\{112\}\langle 110\rangle$ systems to the classical $\{111\}\langle 110\rangle$ ones. In terms of the model proposed above, this neglects the first stages of deformation, when slip occurs only on the $\{111\}$ planes. There are 6 $\{110\}\langle 110\rangle$ systems (plus their opposites), but these systems have to be grouped into 3 pairs. For example, systems $(110)[1\bar{1}0]$ and $(1\bar{1}0)[110]$ constitute one pair, since any strain rate vector which can be accommodated by a given shear rate on one of them can also be accommodated by the same shear rate on the other. In other words, when the components of the vectors N^s associated with each of the

† Instead of constructing the yield surface for all the cases presented below, the linear programming technique was used. Because of the introduction of a hardening law, the maximum work rate (Bishop and Hill) method involves the repeated construction of a new yield surface after each step of the calculation. By contrast, linear programming is considerably more efficient.

systems are written in the 5 dimensional notation described above, it is readily seen that the two vectors coincide, just as the $\{111\}\langle 110\rangle$ systems in fcc materials and the $\{110\}\langle 111\rangle$ systems in bcc materials correspond to the same yield surface. Consequently, it is sufficient to consider only 3 $\{110\}\langle 110\rangle$ systems plus their opposites. However, the activation of one or the other of the two $\{110\}\langle 110\rangle$ systems of a given pair will not lead to the same lattice rotation (Chin and Mammel, 1973); the Chin and Mammel criterion of maximization of colinear slip was therefore used to determine the shear rate on each system of a given pair. This criterion is described in Appendix 2. The other systems which were considered are the $\{112\}\langle 110\rangle$ and there are 12 of these (plus their opposites).

4.3 Prediction of rolling textures

The 3 families of slip systems considered here have 3 different values of $\tau_c : \tau_{c1}$ for the $\{111\}$, τ_{c2} for the $\{110\}$, and τ_{c3} for the $\{112\}$. As a first approximation, $\tau_{c\{hkl\}}$ is equal to 1 when the systems $\{hkl\}\langle 110\rangle$ are assumed to be active and 10 in the opposite case. Five different cases will be treated in turn:

i) $\tau_{c1} = 1$ and $\tau_{c2} = \tau_{c3} = 10$, which is the case when only $\{111\}\langle 110\rangle$ slip is possible (*below* T_1). This case has already been treated in some previous publications (see for example Van Houtte (1981)).

ii) $\tau_{c1} = \tau_{c2} = 1$ and $\tau_{c3} = 10$, where only the $\{110\}\langle 110\rangle$ cross-slip systems are favored ($T_1 < T < T_2$).

iii) $\tau_{c1} = \tau_{c3} = 1$ and $\tau_{c2} = 10$, where only the $\{112\}\langle 110\rangle$ cross-slip systems are favored ($T_1 < T < T_2$).

iv) $\tau_{c1} = \tau_{c2} = \tau_{c3} = 1$, where the three types of system are equally favored ($T_1 < T < T_2$), and

v) $\tau_{c1} = 10$, $\tau_{c2} = \tau_{c3} = 1$, where the cross-slip systems are favored over the conventional slip systems. This corresponds to the temperature range *above* T_2.

Cases (ii) to (v) were tested first in rolling with the FC-RC model (see Section 1) using the linear programming technique. The results are reproduced in Figures 8 to 11 in terms of CODF's for a strain of 3 and a scatter width of 3°. The corresponding {111} pole figures

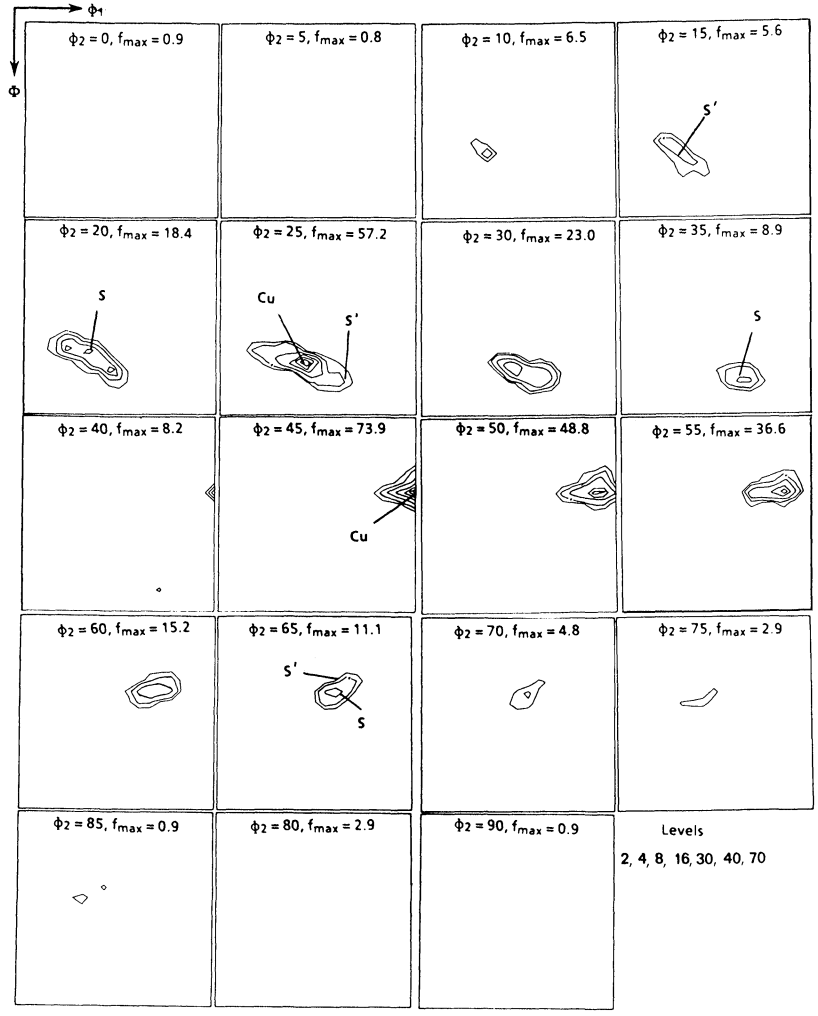

Figure 8 Rolling texture predicted using the FC-RC model with $\{111\} + \{110\}\langle 110\rangle$ slip. $\tau_{c(110)}/\tau_{c(111)} = 1$; $\bar{\varepsilon} = 3$, $\omega_0 = 3°$.

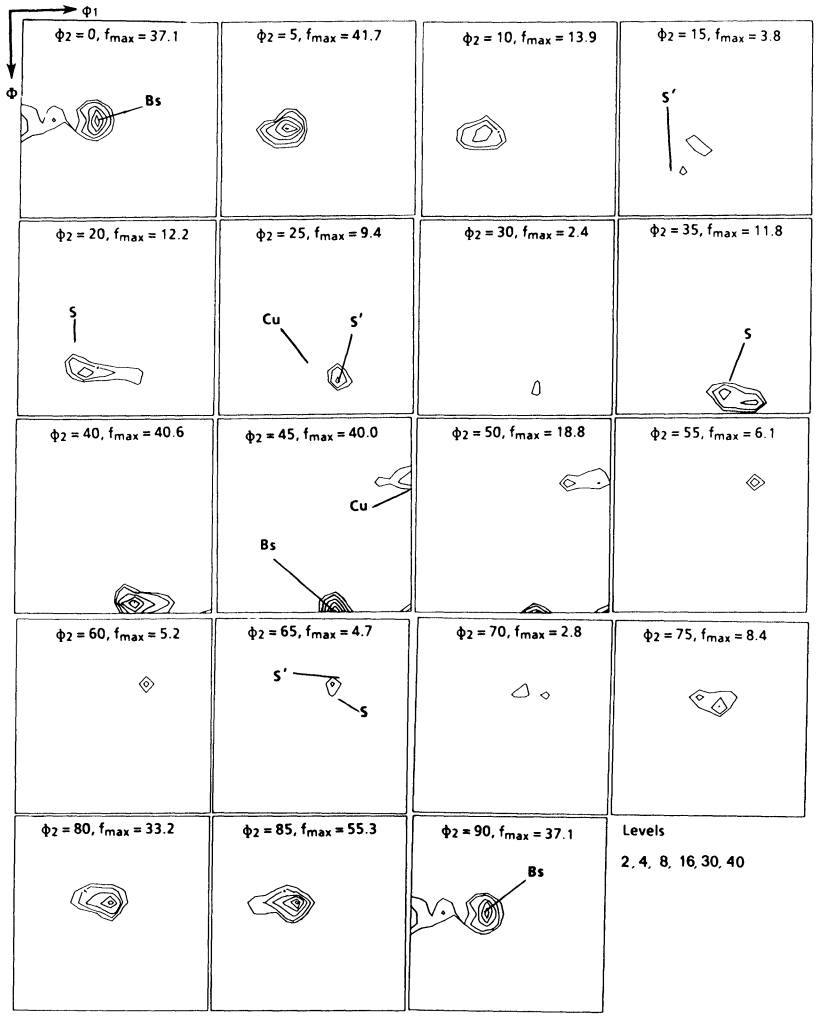

Figure 9 Rolling texture predicted using the FC-RC model with $\{111\} + \{112\}\langle 110\rangle$ slip. $\tau_{c(112)}/\tau_{c(111)} = 1$; $\bar{\varepsilon} = 3$, $\omega_0 = 3°$.

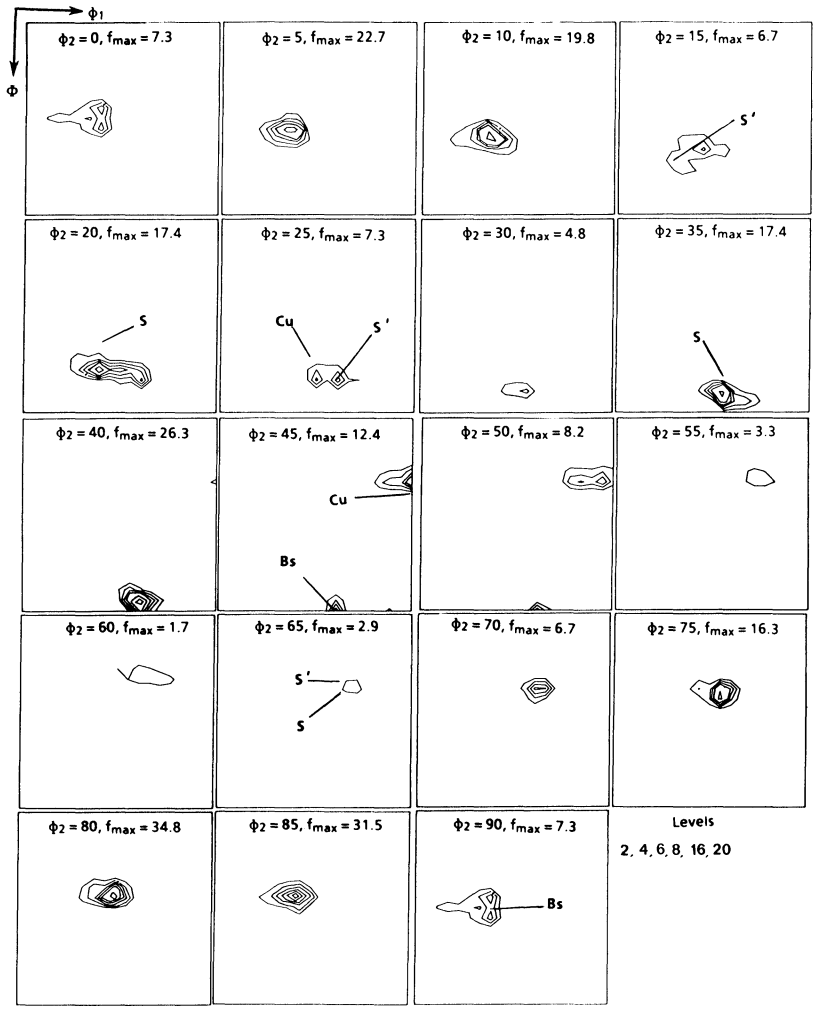

Figure 10 Rolling texture predicted using the FC-RC model with $\{111\} + \{110\} + \{112\}\langle 110\rangle$ slip. $\tau_{c(110)}/\tau_{c(111)} = \tau_{c(112)}/\tau_{c(111)} = 1$; $\bar{\varepsilon} = 3$, $\omega_0 = 3°$.

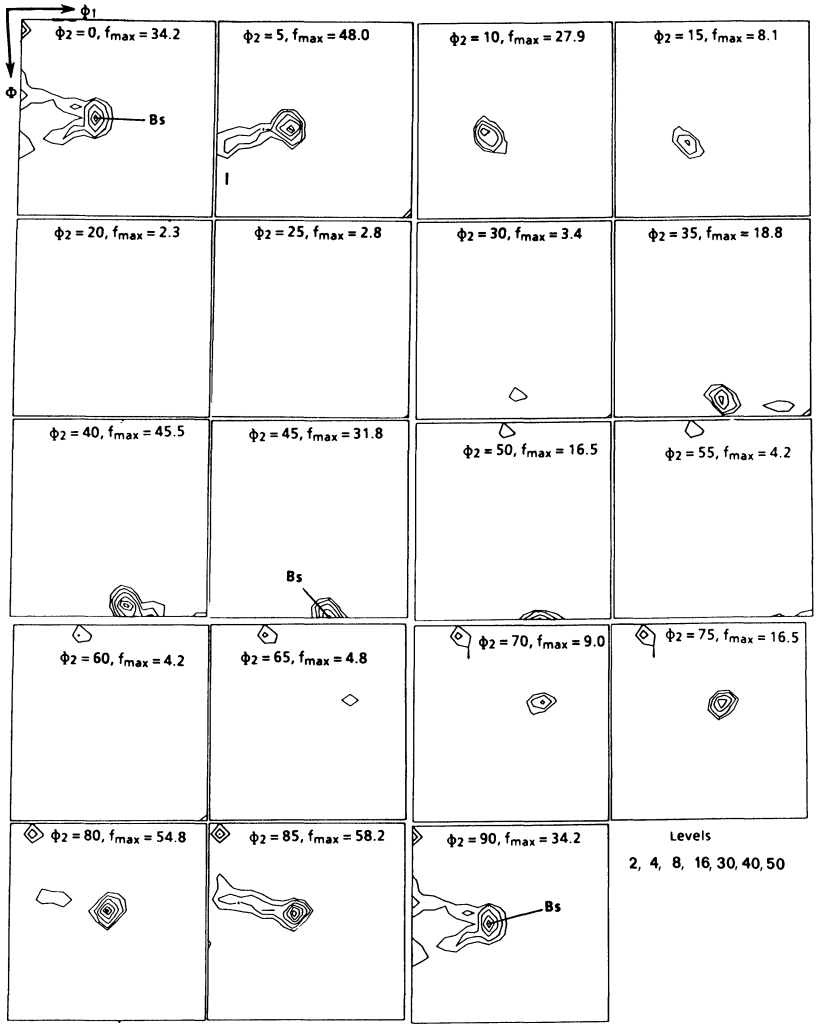

Figure 11 Rolling texture predicted using the FC-RC model with $\{110\} + \{112\}\langle 110\rangle$ slip. $\tau_{c(110)}/\tau_{c(111)} = \tau_{c(112)}/\tau_{c(111)} = 0.1$; $\bar{\varepsilon} = 3$, $\omega_0 = 3°$.

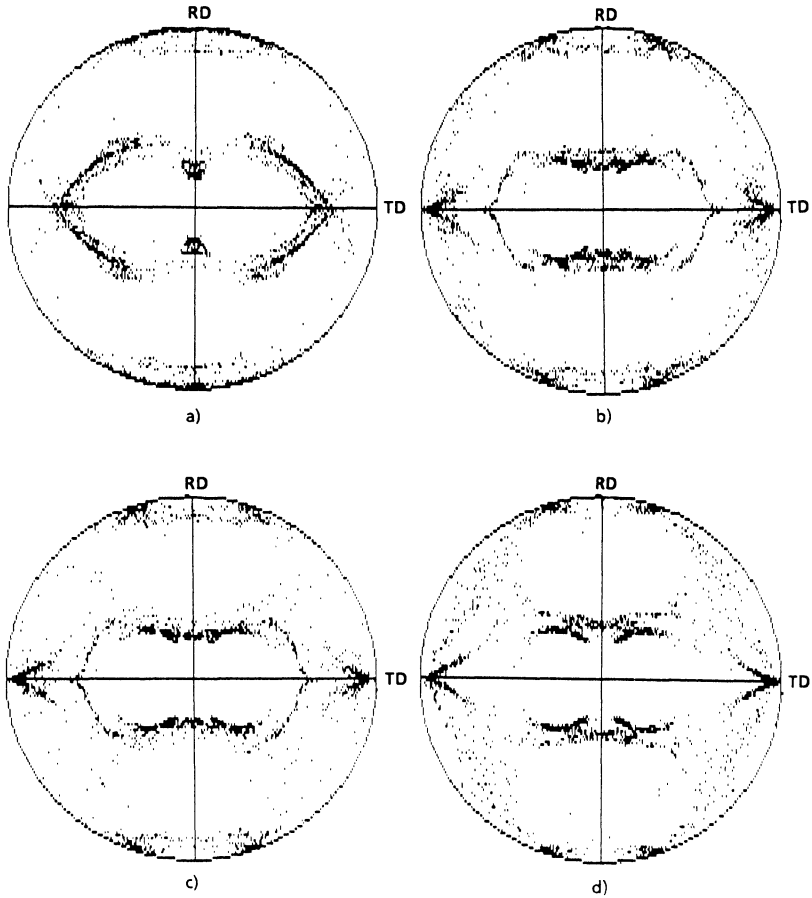

Figure 12 {111} pole figures corresponding to the CODF's presented in Figures 8 to 11; a) {111} + {110} slip, b) {111} + {112} slip, c) {111} + {110} + {112} slip and d) {110} + {112} slip; $\bar{\varepsilon} = 3$.

are presented in Figure 12. It is clear from these figures that every family of slip systems leads to the prediction of different ideal orientations.

In the intermediate range where both slip and cross-slip can occur, the activation of the {111} + {110} systems produces a strong Cu component and a weaker S component (case ii, Figure 8). On the other hand, cross-slip on the {112} planes produces a strong brass component, the Goss and S orientations being much weaker

Table 8 Principal ideal orientations predicted by the FC-RC model with different families of operating slip systems

Possible active slip planes	Predicted ideal orientations
{111}	strong Cu, strong S, weak Goss
{111} + {110}	strong Cu, strong S
{111} + {112}	strong brass, weak Goss and Cu
{111} + {110} + {112}	strong near brass and near Cu
{110} + {112}	strong brass

(case iii, Figure 9). When the two families of cross-slip systems are active concurrently, the ODF can be interpreted in terms of a strong maximum near the brass position, followed by a minor peak near the Cu position (case iv, Figure 10).

When cross-slip alone can take place (case v, Figure 11), only the brass component remains, which is due solely to the activation of the $\{112\}\langle 110\rangle$ systems. It has to be noted that, because of the values of the CRSS's chosen, the $\{112\}\langle 110\rangle$ systems have more influence in these calculations than the $\{110\}\langle 110\rangle$ (see Eq. (11)).

The predicted stable orientations pertaining to the different cases treated above are listed in Table 8. It is worth noting that all the orientations found in rolling over a wide range of SFE and temperature are predicted in one or other of these cases. It can thus be argued that any experimental ODF can be reproduced with the FC-RC model provided that the CRSS's of the cross-slip systems are chosen appropriately. However, perhaps a more physically realistic way of reproducing experimental results would be to introduce hardening laws which can also account for the cross-slip observations of Le Hazif and co-workers (1973, 1975). This is the subject of the section that follows.

5 INTRODUCTION OF LATENT HARDENING

5.1 Theoretical basis

Most latent hardening experiments lead to the conclusion that there is more hardening on the latent systems than on the primary one

(Franciosi, Berveiller and Zaoui, 1980). However, not all the latent systems have the same latent hardening ratio (LHR), although they can be roughly grouped into two categories, depending on their hardening rates:

i) the primary, colinear and coplanar systems, which have low hardening rates; and

ii) the "unrelated" systems, which have high hardening rates (Wierzbanowski and Clément, 1986).

When several systems are active simultaneously, hardening due to slip on all of them has to be taken into account and this can be represented by the following formula:

$$\tau_c^i(t+dt) = \tau_c^i(t) + h_p \sum_j \frac{h_{ij}}{h_p} \dot{\gamma}^j \, dt \tag{12}$$

Here $\tau_c^i(t)$ and $\tau_c^i(t+dt)$ are the values of the CRSS of system i at instant t and at $t+dt$, respectively, $\dot{\gamma}^j$ is the shear rate on system j during the time increment dt, h_p represents the self hardening of the primary systems (set equal for all the systems), and h_{ij} characterizes the interactions between the systems (Franciosi, Berveiller and Zaoui, 1980; Wierzbanowski and Clément, 1986)

To simulate differences in the ease of cross-slip, only colinear systems are considered as low hardening systems in the present case and the values of the h_{ij}/h_p terms can simply be set equal to:

$$\begin{aligned} h_{ij}/h_p &= 1 \quad \text{if } i \text{ and } j \text{ are colinear systems} \\ h_{ij}/h_p &= 1+\beta \quad \text{if } i \text{ and } j \text{ are not colinear} \end{aligned} \tag{13}$$

In the calculations which are presented below, β was set equal to 0.5, which is consistent with previous simulations and published experimental data (Kocks, 1964; Wierzbanowski and Clément, 1986). h_p was set equal to $\tau_{c0\{111\}}$, which implies an approximate increase in the CRSS of 1% for every percent of deformation in a single slip experiment.

With such a simplified hardening law, it is possible to reproduce the experiments described in Refs 12 and 13 by selecting the initial values of the CRSS's of the different systems in such a way that only the $\{111\}\langle 110\rangle$ systems are active at the beginning of the calculation. The CRSS's of the $\{100\}$, $\{112\}$ and $\{110\}\langle 110\rangle$ systems have to be higher than the values given in Eq. (11).

5.2 Predicted rolling textures

As experimental evidence of cross-slip on the {100} planes is less clear than for the other types discussed here, two cases were investigated:

i) $\tau_{c0\{111\}} = 1$, $\tau_{c0\{100\}} = 1.8$, $\tau_{c0\{110\}} = 1.3$, $\tau_{c0\{112\}} = 1.5$, where $\tau_{c0\{hkl\}}$ represents the initial CRSS of the $\{hkl\}\langle 110\rangle$ systems. After a few percent of deformation, any of the above systems can become active; and

ii) $\tau_{c0\{111\}} = 1$, $\tau_{c0\{100\}} = 10$, $\tau_{c0\{110\}} = 1.3$, $\tau_{c0\{112\}} = 1.5$. The high value of τ_c selected for the {100} systems implies that the activation of these systems is essentially forbidden along the entire calculation.

The results of these two simulations are presented in Figures 13 and 14 for an equivalent strain of 3. The Chin criterion of maximization of colinear slip was used for the $\{110\}\langle 110\rangle$ systems and the gaussian spread selected to calculate the CODF is equal to 7° in the two cases. The maxima obtained near the Cu, S and brass positions are listed in Table 9. The results can be interpreted as follows:

When the activation of the $\{100\}\langle 110\rangle$ systems is allowed (Figure 13), the strongest component is again the S (see also Figure 6), whereas the brass is the strongest in the case where cross-slip can only take place on the {112} or {110} planes (see Figure 14).

These results are consistent with the experiments of Le Hazif *et al.* since the activation of these cross-slip planes occurs after a few percent of deformation; they also agree with the experimental textures obtained for aluminum rolled at high temperatures (Bull, 1986). The agreement with experiment is better in the latter case, i.e. when activation of the $\{100\}\langle 110\rangle$ systems is forbidden.

It can be argued that the hardening law selected here is unrealistic and suffers from two important oversimplifications: (i) that the h_{ij} terms are constant with time and stress; and (ii) that only interactions between colinear systems are considered. More realistic laws, such as those quoted by Zarka (1972), Asaro and Needleman (1985), Wierzbanowski *et al.* (1985) and Chidambarrao and Havner (1987), could have been used instead. Nevertheless, the appearance of new texture components is essentially due to allowing

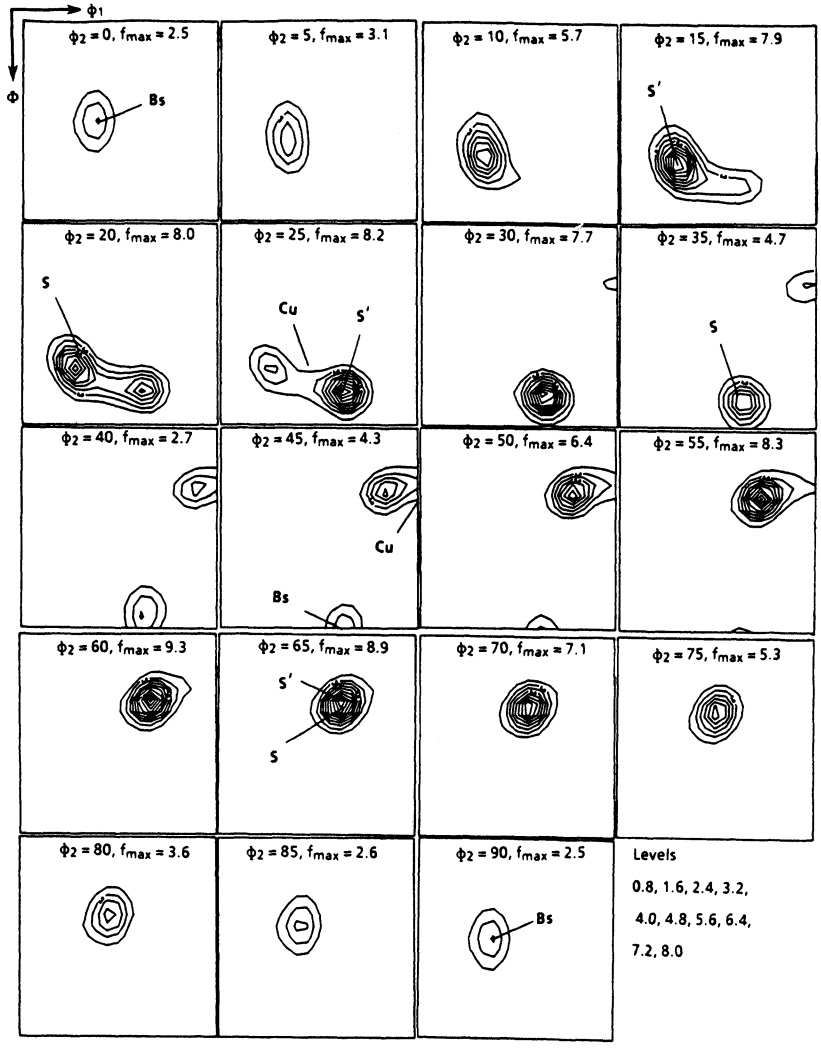

Figure 13 Rolling texture predicted using the FC-RC model with the hardening law defined in Eq. (12) $\bar{\varepsilon} = 3$, $\omega_0 = 7°$, $\tau_{c0\{111\}} = 1$, $\tau_{c0\{100\}} = 1.8$, $\tau_{c0\{110\}} = 1.3$, $\tau_{c0\{112\}} = 1.5$.

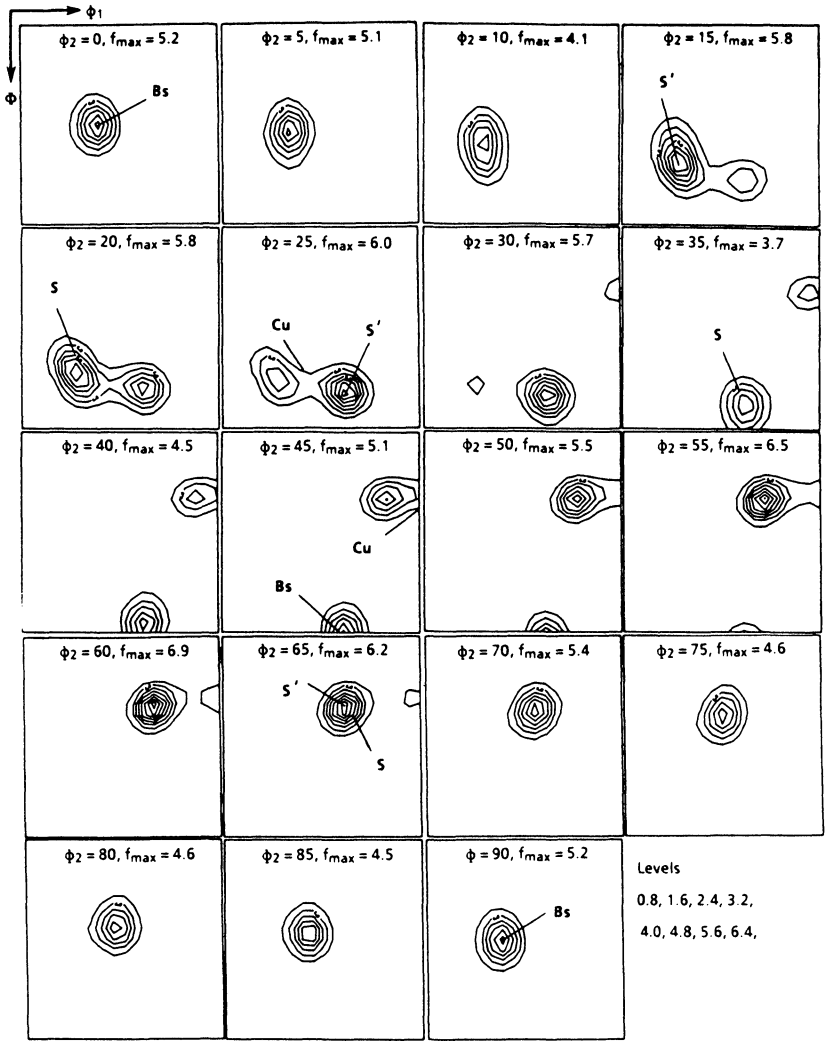

Figure 14 Rolling texture predicted using the FC-RC model with the hardening law defined in Eq. (12). $\bar{\varepsilon} = 3$, $\omega_0 = 7°$, $\tau_{c0\{111\}} = 1$, $\tau_{c0\{100\}} = 10$, $\tau_{c0\{110\}} = 1.3$, $\tau_{c0\{112\}} = 1.5$.

Table 9 Values of the CODF near the brass, Cu and S positions for the textures presented in Figures 13 and 14

Hardening law	brass	Cu	S
with {100}	2.5	6.4	9
without {100}	5.2	5.5	6.2

the values of τ_c on the different systems to vary with time, so that new families of slip systems can become active. Thus the present results are probably qualitatively similar to those that would be obtained with more detailed hardening laws, as long as changes in the relative values of τ_c are permitted.

6. DISCUSSION

6.1 Application to torsion

Several different classes of slip geometry were analyzed above for the case of rolling. Only three of these are presented below for the case of torsion. The four {111} pole figures shown in Figure 15 correspond to the following cases ($\bar{\varepsilon} = 4$):

i) The classical FC-RC model with slip solely on the {111} planes. In this case, the texture is mainly composed of the C orientation $\{100\}\langle 110\rangle$ together with a partial fibre between $A/\bar{A}(\{111\}\langle 110\rangle)$ and $A_1^*(\{\bar{1}11\}\langle 112\rangle)$.

ii) The extreme case of slip solely on the {112} and {110} planes (see Section 4.3, case (v)). Here the $A/\bar{A}$ and A_1^* orientations disappear and there is some spread around the $B/\bar{B}$ position. The C orientation is still very strong.

iii) The hardening law described in Section 5.1 according to which the {100}, {110} and $\{112\}\langle 110\rangle$ systems all become active after the first few increments of strain. Under these conditions, the texture exhibits some scatter around the $A/\bar{A}$ and A_1^* orientations. The concentration is the highest around the $B/\bar{B}$ and C orientations.

iv) The hardening law of Section 5.1, but modified so that slip is forbidden on the {100} planes. Here the texture looks similar to

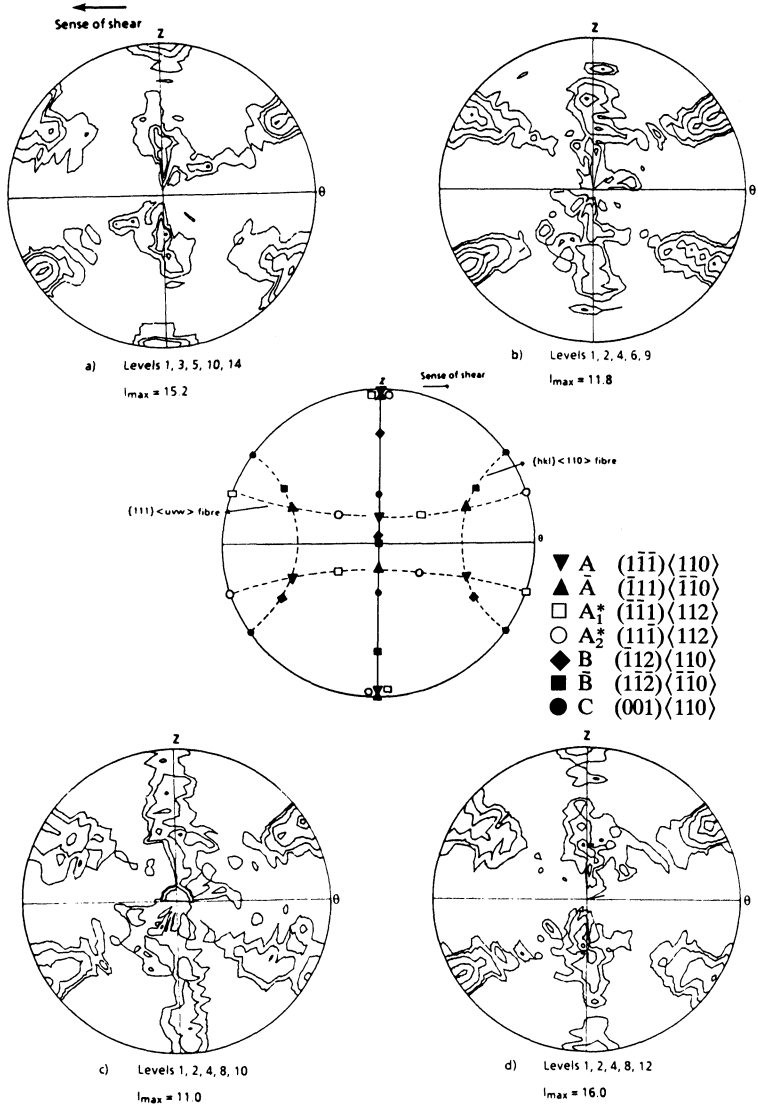

Figure 15 Torsion textures predicted using the FC-RC model for $\bar{\varepsilon} = 4$ with: a) only $\{111\}\langle 110\rangle$ slip, b) only $\{110\} + \{112\}\langle 110\rangle$ cross-slip, c) the hardening law defined in Equation 12 with $\tau_{c0\{111\}} = 1$, $\tau_{c0\{100\}} = 1.8$, $\tau_{c0\{110\}} = 1.3$, $\tau_{c0\{112\}} = 1.5$ and d) the hardening law defined in Eq. (12) with $\tau_{c0\{111\}} = 1$, $\tau_{c0\{100\}} = 10$, $\tau_{c0\{110\}} = 1.3$, $\tau_{c0\{112\}} = 1.5$; $\{111\}$ pole figures.

that of the classical case, but with a slightly higher concentration around $B/\bar{B}$. C is the strongest orientation (as in (i) above) and $B/\bar{B}$ is weaker than in the previous case (iii).

It was seen above that the predicted ideal orientations corresponding to the different families of slip systems are clearly distinguished in rolling. By contrast, the trends are much less clear in the case of torsion, for which an increase in the $B/\bar{B}$ component was expected (Montheillet, Cohen and Jonas, 1984). The strongest peak *near* $B/\bar{B}$ is obtained when the $\{100\} + \{110\} + \{112\}$ systems *all* become active (case iii). This result differs from the rolling case, for which the best agreement was observed when slip is forbidden on the $\{100\}$ planes.

6.2 Limitations of this study

It was seen above that the FC-RC model predicts an increase in the brass component in rolling when new slip or cross-slip systems become activated. The agreement between theory and experiment can even be *quantitatively* satisfactory provided that the CRSS's of the systems are chosen appropriately. However, when this is applied to torsion, the agreement deteriorates. This can be due to one or more of the following reasons:

i) the inappropriateness of the simplified hardening laws that were employed;

ii) the lack of justification for the use of the Chin and Mammel criterion for the maximization of colinear slip;

iii) the irrelevance of the assumptions about grain shape implied by the FC-RC model.

With regard to the latter, it is known that when a polycrystal is deformed at room temperature, the grains become flat and elongated in rolling, whereas they assume a related helical shape in torsion. These special grain shapes permit the relaxation of two shear rates in rolling and one in torsion. However, at high temperatures, a well-formed substructure develops. For example, in torsion, the subgrains are nearly equiaxed and approximately cubic, with faces perpendicular to the sample axes (Ungar *et al.*, 1986). This particular shape calls for the relaxation of *two* shear com-

ponents instead of only one (Kocks and Canova, 1981). Similarly, in rolling, the subgrains are again equiaxed (and of more or less cubic shape), so that all *three* shear components need to be relaxed.†

The influence of enhanced recovery on substructure formation and in this way on the texture developed is too complex a topic for discussion here. It will therefore be treated in greater detail in a separate publication (Bacroix and Jonas, 1987b).

7. CONCLUSIONS

One possible explanation for the differences observed between the high and low temperature deformation textures of fcc metals is that at elevated temperatures there is an increase in the activation of slip or cross-slip systems other than the $\{111\}\langle 110\rangle$. This has sometimes been observed experimentally. The effects of the operation of such mechanisms have been investigated here for the cases of rolling and torsion with the aid of the FC-RC model normally employed at room temperature. Two different methods have been used to introduce the new slip systems:

i) The first consists of setting the CRSS's of the $\{100\}$, $\{110\}$ or $\{112\}\langle 110\rangle$ systems to low enough values so that they can be active concurrently with the $\{111\}\langle 110\rangle$. In this case, either the principle of maximum external work rate, which involves the construction of the mixed polyhedron (Section 2), or the principle of minimum

† A distinction must be made here between small equiaxed grains of various shapes, on the one hand, and equiaxed *and* cubic grains (whose faces are perpendicular to the principal axes of deformation), on the other hand. The former case is generally treated according to the FC model, since the relaxation of any strain rate component involves strong strain rate discontinuities across all the grain boundaries. The latter case has been treated by Kocks and Canova (1981) as being the *least constrained* equiaxed grain case. Since the faces of the cube are perpendicular to the principal axes of deformation, compatibility requires the principal components of the strain rate to be continuous through *all* the boundaries. One additional shear component has to be continuous through each boundary, different for each type of face. Thus, the assumption that the principal strain rates are constant throughout each grain (and consequently throughout all the grains) satisfies the most important compatibility relations everywhere. The additional adjustments necessary in the neighborhood of grain boundaries generally average out to give zero macroscopic shear in accordance with the specimen symmetry.

internal work rate, with the aid of the linear programming technique (Section 4), can be used.

ii) The second consists of employing a latent hardening law which assumes that the CRSS's of the different systems are *not* constant. Consequently, even if the initial values are such that only the $\{111\}\langle 110\rangle$ systems are active at the beginning of the simulation, other systems can become active due to differential hardening of the different systems. The law selected in this study only took into account interactions between colinear systems.

From this study, the following conclusions can be drawn:

1) In rolling, the activation of the $\{100\}\langle 110\rangle$ systems leads to the prediction of a strong S component, whereas slip on the $\{110\}$ planes produces mainly a Cu component and slip on the $\{112\}$ planes a brass-type texture.

2) When all the systems are concurrently active (through the use of the latent hardening law), the three components are present simultaneously, in proportions which vary with the ratios of the initial CRSS's. By contrast, the brass component is completely absent from the FC-RC predictions when only slip on the $\{111\}$ planes is considered. Consequently, the present results are in good agreement with high temperature rolling textures, in which the brass component is in fact present (Bacroix and Jonas, 1987a).

3) The results are not quite so clear in the case of torsion. On the basis of the rolling results, the intensity of the $B/\bar{B}$ (brass) orientation was expected to increase; however, the predicted increase at $\bar{\varepsilon} = 4$ is relatively small when compared with the results of the classical FC-RC model, in which slip can only take place on the $\{111\}$ planes.

4) The poor agreement in torsion may be due to the relatively small strains involved in the simulations or to the effects of enhanced recovery and the presence of an equiaxed substructure. In the latter case, the components of the strain rate tensor which can be relaxed in each grain or subgrain must be modified. When the recovery processes leading to substructure formation are properly taken into account, better predictions are indeed obtained (Bacroix and Jonas, 1987a).

Acknowledgements

The authors are indebted to Dr P. Gilormini for his help in the treatment of the CODF's as well as to Drs J. H. Driver, R. Fortunier, Ph. Lequeu and F. Montheillet for making a number of fruitful suggestions during the course of this work. They also acknowledge with gratitude the financial support received from the Natural Sciences and Engineering Research Council of Canada, the Quebec Ministry of Education (FCAR program), and the Canadian Steel Industry Research Association.

References

Asaro, R. J. and Needleman, A. (1985). Texture development and strain hardening in rate dependent polycrystals. *Acta Metallurgica,* **33,** 923–953.

Bacroix, B. (1986). *Prediction of high Temperature Deformation Textures in Fcc Materials.* Ph.D. Thesis, McGill University, Montreal.

Bacroix, B. and Jonas, J. J. (1987a). Influence of temperature on deformation textures in fcc metals. In *Proc. ICOTOM 8,* Santa Fe, New Mexico, Sept., 1987.

Bacroix, B. and Jonas, J. J. (1987b). To be published.

Barrett, C. S. and Massalski, T. B. (1966). *The Structure of Metals: Crystallographic Methods, Principles and Data,* 3rd edn, McGraw Hill Book Company, New York.

Bull, M. (1986). Private communication. Alcan Research Laboratories, Kingston, Ontario.

Canova, G. R., Kocks, U. F. and Jonas J. J. (1984). Theory of torsion texture development. *Acta Metallurgica,* **32,** 211–226.

Chidambarrao, D. and Havner, K. S. (1987). Finite deformation analysis of fcc crystals in (110) $(1\bar{1}2)$ $(\bar{1}11)$ channel die compression. Submitted to *International Journal of Plasticity.*

Chin, G. Y. and Mammel, W. L. (1967). Computer solutions of the Taylor analysis for axisymmetric flow. *Transactions of the Metallurgical Society of AIME,* **239,** 1400–1405.

Chin, G. Y. and Mammel, W. L. (1973). A theoretical examination of the plastic deformation of ionic crystals: II. Analysis of uniaxial deformation and axisymmetric flow for slip on $\{110\}\langle 110\rangle$ and $\{100\}\langle 110\rangle$ systems. *Metallurgical Transactions,* **4,** 335–340.

Franciosi, P., Berveiller, M. and Zaoui, A. (1980). Latent hardening in copper and aluminum single crystals. *Acta Metallurgica,* **28,** 273–283.

Grewen, J. and Wasserman, G. (1969). *Textures in Research and Practice,* Springer, Berlin.

Hirsch, J. (1984). Waltztexturentwicklung in Kubisch-Flächenzentrierten Metallen. Ph.D. Thesis, Aachen, Germany.

Hirth, J. P. and Lothe, J. (1968). *Theory of Dislocations,* McGraw Hill, New York.

Honneff, H. and Mecking, H. (1978). A method for the determination of the active slip systems and orientation changes during single crystal deformation. In *Proc. ICOTOM 5,* edited by G. Gottstein and K. Lücke, pp. 265–275, Vol. I, Aachen, Germany.

Hu, H., Cline, R. S. and Goodman, S. R. (1966). Deformation textures of metals. In *Recrystallization, Grain Growth and Textures,* pp. 295–367. ASM, Metals Park, Ohio.

Ito, K., Müsik, R. and Lücke, K. (1983). The influence of iron content and annealing temperature on the recrystallization textures of high purity aluminum-iron alloys. *Acta Metallurgica,* **31,** 2137–2149.

Kocks, U. F. (1964). Latent hardening and secondary slip in aluminium and silver. *Transactions of the Metallurgical Society of AIME,* **230,** 1160–1167.

Kocks, U. F. and Canova, G. R. (1981). How many slip systems and which?. In *Deformation of Polycrystals: Mechanisms and Microstructures,* edited by Hansen *et al.,* pp. 35–44. Proc. of 2nd RISØ International Symposium.

Kocks, U. F., Canova, G. R. and Jonas, J. J. (1983). Yield vectors in fcc crystals. *Acta Metallurgica,* **31,** 1243–1252.

Leffers, T. (1981). The {111} rolling texture component in brass and its relation to the formation of the brass-type texture. In *Proc. ICOTOM 6,* edited by S. Nagashima, pp. 385–395. ISIJ, Tokyo, Japan.

Le Hazif, R., Dorizzi, P. and Poirier, J. P. (1973). Glissement $\{110\}\langle 110\rangle$ dans les métaux de structure cubique à faces centrées. *Acta Metallurgica,* **21,** 903–912.

Le Hazif, R. and Poirier, J. P. (1975). Cross-slip on {110} planes in aluminum single crystals compressed along $\langle 100\rangle$ axis. *Acta Metallurgica,* **23,** 865–871.

Lequeu, Ph., Gilormini, P., Montheillet, F., Bacroix, B. and Jonas, J. J. (1987). Yield surfaces for textured polycrystals. I. Crystallographic approach. *Acta Metallurgica,* **35,** 439–451.

Lücke, K., Pospiech, J., Virnich, K. H. and Jura, J. (1981). On the problem of the reproduction of the true orientation distribution from pole figures. *Acta Metallurgica,* **29,** 167–185.

Mecking, H. (1985). Textures in metals. In *Preferred Orientation in Deformed Metals and Rocks: An Introduction to Modern Texture Analysis,* edited by H. R. Wenk, pp. 267–306. London, Academic Press.

Montheillet, F., Cohen, M. and Jonas, J. J. (1984). Axial stresses and texture development during the torsion testing of Al, Cu and α-Fe. *Acta Metallurgica,* **32,** 2077–2089.

Orlans-Joliet, B., Bacroix, B., Montheillet, F., Driver, J. H. and Jonas, J. J. (1987). Yield surfaces of bcc crystals for slip on the $\{110\}\langle 111\rangle$ and $\{112\}\langle 111\rangle$ systems. Submitted to *Acta Metallurgica.*

Smallman, R. E. (1955–56). Textures in face-centred cubic metals and alloys. *Journal of the Institute of Metals,* **84,** 10–18.

Taylor, G. I. (1938). Plastic strain in metals. *Journal of the Institute of Metals,* **62,** 307–324.

Tomé, C. N., Canova, G. R., Kocks, U. F., Christodoulou, N. and Jonas, J. J. (1984). The relation between macroscopic and microscopic strain hardening in fcc polycrystals. *Acta Metallurgica,* **32,** 1637–1653.

Tomé, C. N. and Kocks, U. F. (1985). The yield surface of hcp crystals. *Acta Metallurgica,* **33,** 603–621.

Ungar, T., Toth, L. S., Illy, J. and Kovacs, I. (1986). Dislocaton structure and work hardening in polycrystalline OFHC copper rods. *Acta Metallurgica,* **34,** 1257–1267.

Van Houtte, P. (1981). Adaptation of the Taylor theory to the typical substructure of some cold rolled fcc metals. In *Proc. ICOTOM 6,* edited by S. Nagashima, pp. 428–437. ISIJ, Tokyo, Japan.

Wierzbanowski, K. (1978). Computer simulation study of texture transitions in fcc metals and alloys. In *Proc. ICOTOM, 5,* Vol. I, edited by G. Gottstein and K. Lücke, pp. 309–317. Aachen, Germany.

Wierzbanowski, K. and Clément, A. (1986). Exemple d'application de la program-

mation linéaire à la plasticité des métaux. *Mémoires et Etudes scientifiques Revue de Métallurgie,* 83, 161–167.
Wierzbanowski, K., Hihi, A., Berveiller, M. and Clément, A. (1984). Rolling textures predicted by self consistent model and continuity equation. In *Proc. ICOTOM 7,* edited by C. M. Brakman *et al.*, pp. 179–184. Noordwijkerhant, Holland.
Zarka, J. (1972). Généralisation de la théorie du potentiel plastique multiple en viscoplasticité. *Journal of the Mechanics and Physics of Solids,* **20,** 179–195.

APPENDIX 1

Calculation of the CODF for ideal orientations with a gaussian scatter

When a texture is composed of only one ideal orientation g_0, around which the scatter is represented by a gaussian distribution, the CODF $f(g)$ is given by (Lücke *et al.*, 1981):

$$f(g) = S_0 \exp(-\omega^2/\omega_0^2) \tag{A1.1}$$

with

$$S_0 = \frac{2\sqrt{\pi}}{Z_0\omega_0[1 - \exp(\omega_0^2/4)]} \tag{A1.2}$$

In these equations, ω_0 is the spread around g_0, ω is the misorientation between g and g_0 and Z_0 is the so-called multiplicity of the orientation g_0. It represents the number of points that describe the orientation g_0 in Euler space and depends on both the crystal and sample symmetries. For most orientations, Z_0 is equal to 96 in the case of rolling, but can be reduced to 48 or 24 in the case of symmetrical orientations. For example, Z_0 is 48 for the Cu and brass orientations and 24 for the cube component.

Once ω_0 has been selected and Z_0 determined, $f(g)$ can be calculated from relation A1.1 through the following formula for ω:

$$1 + 2\cos\omega = \max(\text{trace}(g_0 \cdot {}^t g_e)) = \max(\text{trace}(g_{0e} \cdot {}^t g)). \tag{A1.3}$$

Here g_{0e} and g_e represent the orientations which are equivalent to g_0 and g, respectively, when both the crystal and sample symmetries are taken into account. Only one of the two kinds of products listed in Eq. (A1.3) needs to be calculated.

When the texture is composed of N ideal orientations g_{0i}, each of which is characterized by a particular gaussian spread ω_{0i} and a multiplicity Z_{0i}, the CODF is given by:

$$f(g) = \frac{1}{N} \sum_{i=1}^{N} S_{0i} \exp(-\omega_i^2/\omega_{0i}^2) \tag{A1.4}$$

with

$$S_{0i} = \frac{2\sqrt{\pi}}{Z_{0i}\omega_{0i}[1 - \exp(\omega_{0i}^2/4)]} \tag{A1.5}$$

In this case, Z_{0i} must first be calculated for every g_{0i}, and ω_i can be determined for each point g in Euler space and every g_{0i} with the aid of equation A1.3. This procedure is very simple and does not involve any development of the CODF in the form of spherical harmonics; it also gives the exact value of the CODF for a gaussian distribution. The only drawback is the length of the calculation, since 96 products $g_0 \cdot {}^t g_e$ need to be evaluated for each g and g_{0i}. This is nevertheless readily handled by any microcomputer.

APPENDIX 2

The maximization of colinear slip

In the case of the $\{110\}\langle 110\rangle$ systems, the vectors n and b define a *pair* of slip systems n_1, b_1, and n_2, b_2 with:

$$\begin{aligned} n_1 &= n, \qquad b_1 = b \\ n_2 &= b, \qquad b_2 = n \end{aligned} \tag{A2.1}$$

where n_1 and n_2 are the slip plane normals and b_1 and b_2 are the slip directions. (This is because the index 110 can refer to both a slip direction *and* a slip plane.) Generally, when several systems are active, minimization of the internal work rate gives the value of the shear rate $\dot{\gamma}^s$ on *every* active slip system. However, when one of the systems corresponds to the $\{110\}\langle 110\rangle$ pair considered here, only the sum $\dot{\gamma}_1 + \dot{\gamma}_2$ can be determined, where $\dot{\gamma}_1$ is the shear rate on system n_1, b_1 and $\dot{\gamma}_2$ the shear rate on system n_2, b_2. If $\dot{G}_1$ and $\dot{G}_2$ designate the sum of the shear rates on the other *active* systems

having b_1 and b_2 as their slip directions, respectively, the activity of the colinear systems can be maximized by simply letting $\dot{\gamma}_1$ and $\dot{\gamma}_2$ be proportional to $\dot{G}_1$ and $\dot{G}_2$, respectively (Chin and Mammel, 1973). The rules are the following:

$$\dot{G}_1 + \dot{G}_2 = 0 \Rightarrow \dot{\gamma}_1 = \dot{\gamma}_2 = \tfrac{1}{2}(\dot{\gamma}_1 + \dot{\gamma}_2)$$

$$\dot{G}_1 + \dot{G}_2 \neq 0 \Rightarrow \dot{\gamma}_1 = \frac{\dot{G}_1}{\dot{G}_1 + \dot{G}_2}(\dot{\gamma}_1 + \dot{\gamma}_2) \quad \text{and} \quad \dot{\gamma}_2 = \frac{\dot{G}_2}{\dot{G}_1 + \dot{G}_2}(\dot{\gamma}_1 + \dot{\gamma}_2) \tag{A2.2}$$

The first condition applies when none of the active systems, except for the $\{110\}\langle 110\rangle$ system, has b_1 or b_2 as a slip direction. In this case, neither of the two systems of the 110 pair can be preferred, and the two have equal shear rates. In the remaining case, the shear rate is the greater along the slip direction which is already the one most activated by the other systems.